Flexible connectivity under physiological constraints

Gabriel Koch Ocker[*1], Michael A. Buice[**1,2]

1 Allen Institute for Brain Science, Seattle, WA, USA
2 Department of Applied Mathematics, University of Washington, Seattle, WA, USA
* gabeo@alleninstitute.org
** michaelbu@alleninstitute.org

Abstract

Physiological constraints define allowed configurations of synaptic weights for neural circuits. How this affects circuit function remains little understood. We examine the hypothesis that neural circuits may be structured to make constraints flexible: to allow many configurations of synaptic weights. The size of these allowed weight spaces depends on the number of inputs to a neuron: its connectivity degree. We predict degree distributions that optimize simple constraints on a neuron's total synaptic weight. We also find the degrees of connectivity that maximize the number of allowed synaptic weight configurations. To test these predictions, we examine reconstructions of the mushroom bodies from the first instar larva and the adult *Drosophila melanogaster*. Overall, flexibility under a homeostatically fixed total synaptic weight describes Kenyon cell connectivity better than other models, suggesting a principle shaping the apparently random structure of Kenyon cell wiring.

1 Introduction

The connectivity of neural circuits, together with neurons' intrinsic dynamics, determines their computation. These computations are most easily specified close to the periphery. For example, synaptic connectivity within the retina underlies direction selectivity computations [4, 25, 56] and olfactory receptor expression determines projection patterns from olfactory receptor neurons to glomeruli, underlying a combinatorial code for odorants [29, 41, 47, 57–59]. In more central neurons, computations can be shaped by experience-dependent plasticity. For example, random connectivity in cerebellar and cerebral cortices may form high-dimensional representations to facilitate associative learning and linear readout [1, 40], and cortical pyramidal neurons may optimally store uncorrelated input patterns [5, 9, 44].

Neuronal connectivity is also homeostatically regulated and constrained by physiological limits. The total strength of synaptic connections between two neurons is limited by the amount of receptor and neurotransmitter available and the size of the synapse [31]. Pyramidal neurons of the cortex and hippocampus undergo synaptic scaling, regulating their total excitatory [16, 20, 21, 53] and inhibitory [23, 30, 33, 39, 54] synaptic input strengths to regulate postsynaptic activity levels [26]. In *Drosophila melanogaster*, growth from the first instar larva to the third instar larva is accompanied by a homeostatic regulation of mechanosensory receptive fields [22] and functional motor neuron outputs [32] and nociceptive projections [19]. In addition, changes in inputs to the central aCC neuron elicit structural modifications to its dendritic tree that homeostatically maintain input levels [51].

Despite its constraints, neural connectivity must enable computation. Learning, furthermore, requires changes in synaptic weight configurations. In models of associative memory, different configurations of synaptic weight correspond to distinct memories [28]. We reasoned that in order for the constraints to interfere minimally with computation and, moreover, to facilitate as wide an array of learned computations as possible, neural connectivity should have evolved to maximize the total number of configurations available under physiological constraints. That is, the circuit might have evolved to be flexible. A tight constraint defines a small space of allowed weight configurations (Fig. 1a), while a flexible one defines a large space of allowed weight configurations (Fig. 1b). We measure the flexibility of a constraint by the number of synaptic weight configurations that it allows.

We asked what patterns of neural connectivity maximize the number of possible weight configurations. Based on this optimization principle, we derive a distribution for the total number of synaptic partners to any given neuron subject solely to a specific constraint. We found that for constraints on a neuron's net synaptic weight (either input or output), the mode of this distribution is characterized by a nearly linear relation between the net synaptic weight and the number of presynaptic partners. This holds for both homeostatically fixed net weights and for a maximal net weight.

We test our theory using recently available wiring diagrams of an associative learning center in *Drosophila melanogaster*, the larval [18] and adult [50] mushroom bodies, where a combinatorial code for odorants in Kenyon cells (KCs) [7, 42, 49] forms a substrate for associative learning at output neurons [24, 48]. In the larva, we find that the input and output connectivity of immature (unclawed) Kenyon cells (MCs) best matches the optimally flexible configurations. In the adult, the alpha prime Kenyon cells best matches the optimally flexible configurations. The two constraints, fixed net weights and maximal net weights, each predict a distribution for the degrees. We performed a Bayesian analysis to compare these with a binomial random wiring model. We found that overall, the fixed net weight model provided the best description for Kenyon cell connectivity, with the single exception of mature KCs in the larva, suggesting a developmental progression between principles governing random KC wiring in the larva.

2 Results

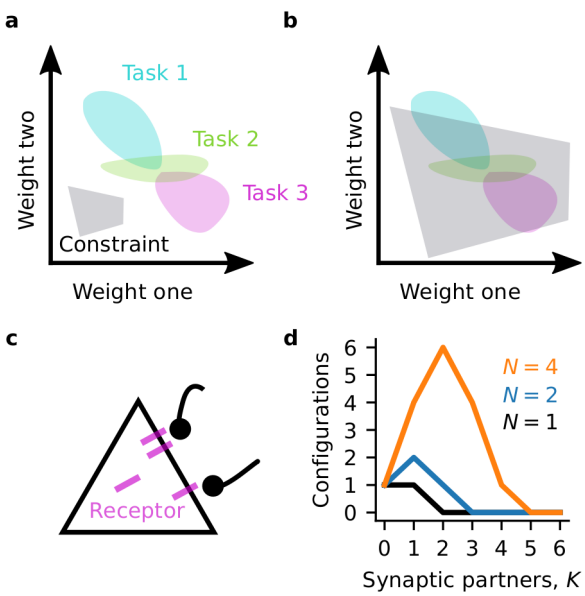

Fig 1. Constraints on synaptic connectivity. (**a**) Synaptic weights occupy a K-dimensional space. K is the number of synaptic partners. The solution spaces for computational tasks are subspaces of the synaptic weight space, with dimension up to K. Constraints also define subspaces with dimension up to K. A tight constraint defines a small subspace with potentially low overlap with computational solution spaces. (**b**) A loose constraint defines a large subspace, with greater potential overlap with computational solution spaces. (**c**) A neuron that has $N = 4$ units of synaptic weight (here, receptors) to distribute amongst two synaptic partners and a pool of unused synaptic weight. (**d**) Number of possible connectivity configurations for different values of K and N (given by the binomial coefficient).

2.1 Measuring constraint flexibility

We begin with a simple example where a neuron has N units of synaptic weight, of size ΔJ, available. These could correspond, for example, to individual receptors or vesicles. It can assign these synaptic weight units to its K partners (presynaptic partners as in Fig. 1c for receptors, or postsynaptic partners for vesicles). We can count how many this constraint can be satisfied. If not all synaptic weight units have to be assigned, we can consider $K + 1$ partners (the additional partner corresponding to unused synaptic weight units). For $N = 4$ and two connections, there are six possible configurations. With three connections, there are four possible configurations. Thus with the constraint of $N = 4$, three connections are more flexible than two since there are more ways to satisfy the constraint. Since the constraint treats all synaptic partners symmetrically, the number of possible

configurations is given by the binomial coefficient "N choose K". For different numbers of synaptic weight units N, there are different maximally flexible configurations K (Fig. 1d).

In many neural circuits, connections between neurons can take on different strengths or weights. We consider a simple model of synaptic interactions where a neuron has K synaptic partners and the total strength of projection i is J_i. Synaptic weights can be made up of many small units of strength, corresponding to (for example) individual receptors or vesicles. In this case, it is reasonable to model individual synaptic weights as continuous variables. We can visualize these weights as a vector in the K-dimensional synaptic weight space; K is the synaptic degree. These partners could be either all presynaptic, or all postsynaptic. A particular configuration of synaptic weights occupies a point in the K-dimensional synaptic weight space. Different computational tasks for the neuron specify solution spaces for the synaptic weight vectors (Fig. 1a). A constraint specifies a space of allowed synaptic weights. We will examine the hypothesis that synaptic connectivity is structured to make these spaces large: to make the constraint flexible.

2.2 Flexibility under bounded net synaptic weight

We begin by considering an upper bound on the net synaptic weight, so that

$$\sum_{i=1}^{K} J_i \leq \bar{J} \tag{1}$$

This bound could be interpreted multiple ways, for example as a presynaptic limit due to the number of vesicles currently available before more are manufactured or a postsynaptic limit due to the amount of dendritic tree available for synaptic inputs.

With K synaptic partners, the constraint (1) defines a volume in K dimensions. For a neuron with two synaptic partners, this is the portion of the plane bounded by the axes and a line that stretches between them (Fig. 1a). For three synaptic partners, the weights live in three-dimensional space and are constrained to lie in the volume under an equilateral triangle (Fig. 1b). (It is equilateral because its vertices are defined by the configurations where one connection uses the total weight, $\bar{J}$.) In general, for K synaptic partners the synaptic weights live in the volume under a $K-1$ dimensional simplex in K-dimensional synaptic weight space. Thus, for the bounded weight constraint the number of weight configurations is proportional to the volume of the $K-1$ dimensional simplex, V:

$$V(K, \bar{J}) = \frac{\bar{J}^K}{K!} \tag{2}$$

We can also view this as a count of available configurations if we divide the maximum synaptic weight $\bar{J}$ into N increments of measurable synaptic weight changes ΔJ, and measure synaptic weights relative to ΔJ (replacing $\bar{J}$ with $\bar{J}/\Delta J = N$). For large N, the volume under the simplex approximates the number of synaptic weight configurations (Methods: 6.1).

The volume under the simplex increases with the max weight $\bar{J}$, but for $\bar{J} \geq 2$ it has a maximum at $K > 1$ (Fig. 1c). Our hypothesis is that this could serve as an objective function for circuit connectivity optimization. We consider a population of neurons, each performing this optimization with variable success. If our only information about circuit connectivity is the constraint, Eq. 1, and all synaptic weight configurations satisfying it have equal prior likelihood, this defined a matching distribution for circuit connectivity, p_V. That is, degrees of connectivity should have observed frequencies proportional to the size of the constraint space they define. These frequencies will depend also on the total available synaptic weight of each neuron. In total, this implies that

$$p_V(K|\bar{J}) = \frac{V\left(K, \bar{J}\right)}{Z_V(\bar{J})} \tag{3}$$

where Z_V is a normalization constant that ensures that the distribution sums to 1. (For the bounded weight constraint, that normalization constant is $-1 + \exp \bar{J}$ and p_V is a zero-truncated Poisson distribution.) Before analyzing distributions of connectivity, we ask what connectivity maximizes the size of this constraint space.

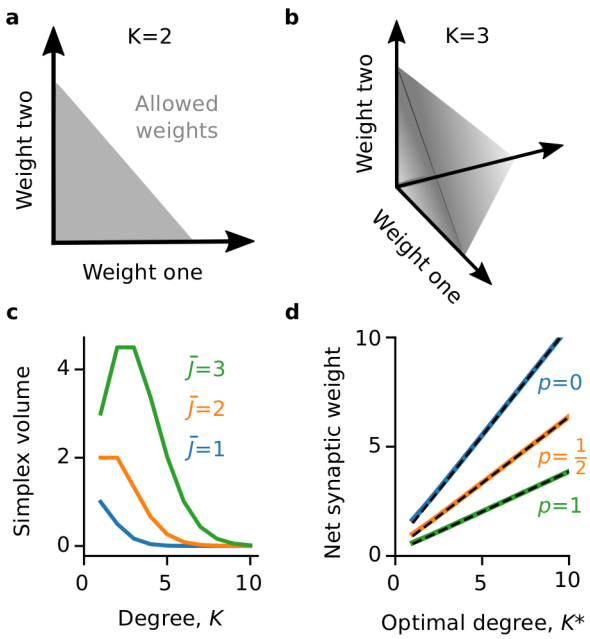

Fig 2. Size of the synaptic weight space with bounded total input. (**a**) For two inputs, the synaptic weights must live in the area under a regular 1-simplex. (**b**) For three inputs, the synaptic weights must live in the volume under a regular two-simplex. (**c**) Volume of the $K-1$ simplex as a function of the number of presynaptic partners, K, for different maximal net weights $\bar{J}$. (**d**) Relation between the in-degree that maximizes the simplex volume, K^*, and the net synaptic weight, $(K^*)^p \bar{J}$. Solid lines: theoretical prediction; dashed black lines: linear approximation.

We call the synaptic degree that maximizes the volume under the simplex the optimal degree, K^*. We computed this optimal degree to get the mode of the distribution (Methods 6.2). It is approximately linearly related to the total synaptic weight:

$$\bar{J} = K^* + \frac{1}{2} + \mathcal{O}\left(1/K^*\right) \tag{4}$$

where $\mathcal{O}\left(1/K^*\right)$ denotes terms proportional to $1/K^*$ or higher powers of $1/K^*$. We generalized these analyses to allow the maximum synaptic weight to depend on the number of synapses:

$$\sum_{j=1}^{K} J_j \leq K^p \bar{J} \tag{5}$$

for some power p. This scaling of the summed synaptic weight corresponds to scaling the individual synaptic weights as K^{p-1}. If every synaptic weight has an order $1/K$ strength, the sum of the synaptic weights would be order 1 and $p = 0$. If every synaptic weight has an order 1 strength, the summed weight is order K and $p = 1$. If synaptic weights have balanced $(1/\sqrt{K})$ scaling [55], then the summed weight would have $p = 1/2$. This replaces the maximum weight $\bar{J}$ with $K^p \bar{J}$ in the formulas for the volume under the simplex and its accompanying distribution, Eqs. 1, 3.

In general, for the mode of the distribution we found (Methods 6.3) an approximately linear relation between the maximum synaptic weight $K^p \bar{J}$ and the optimal in-degree K^* for any p:

$$(K^*)^p \bar{J} = \left(K^* + \frac{1}{2}\right) \exp\left(-p\right) + \mathcal{O}\left(1/K^*\right) \tag{6}$$

If $p = 0$, this reduces to Eq. 4. We can see from Eq. 6 that if $p = 1$, we obtain the condition $\bar{J} = 1/e$ (to leading order). So if $p = 1$ and $\bar{J} = 1/e$, the surface area is approximately independent of K. If $p = 1$ and $\bar{J} < 1/e$, the

volume decreases monotonically and vice versa. These predictions for the optimal degree correspond to predictions for the mode of the predicted degree distribution, Eq. 3.

2.3 Flexibility under fixed net synaptic weights

Motivated by the observation that different types of neuron regulate their total excitatory synaptic weight [52], we also consider a simple model of homeostatic synaptic scaling:

$$\sum_{j=1}^{K} J_j = K^p \bar{J} \tag{7}$$

where the net synaptic weight is fixed at $K^p\bar{J}$. As above, We again consider the total synaptic weight to be composed of many small increments, so that it is reasonable to model synaptic weights as taking continuous values.

Our reasoning here follows that from the bounded weight constraint. For two synaptic weights, the fixed weight constraint also defines a line in the plane of synaptic weights that synaptic weights must live on (Fig. 1a). For three inputs, the constraint space is the surface of an equilateral triangle (Fig. 1b). In general, the fixed net weight constraint defines the same geometric objects as the bounded net weight, but requires synaptic weights to live on their surfaces instead of the volumes under them. The size of the space of allowed weights under Eq. 7 is given by the surface area of the $K-1$ simplex, A:

$$A(K, \bar{J}) = \frac{\left(K^p \bar{J}\right)^{K-1} \sqrt{K}}{(K-1)!} \tag{8}$$

and, similarly to the bounded weight constraint, we hypothesize an optimization that favors this area so that the probability of K synaptic partners is given by

$$p_A(K|\bar{J}) = \frac{A\left(K, \bar{J}\right)}{Z_A(\bar{J})} \tag{9}$$

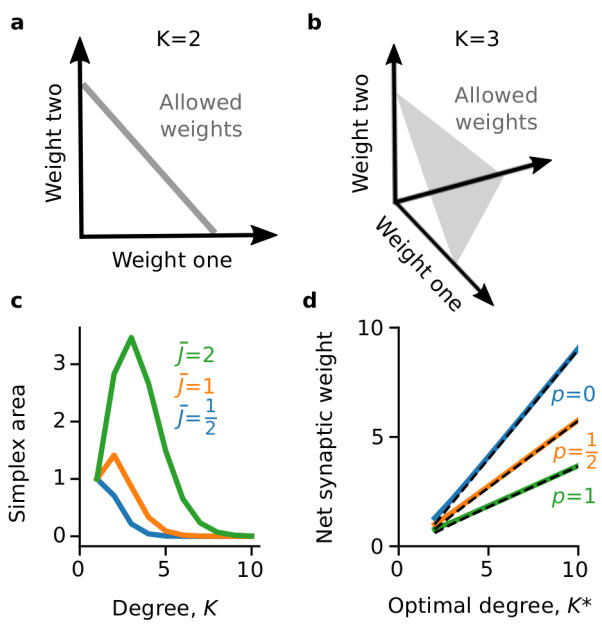

Fig 3. Size of the synaptic weight space with fixed total excitatory weight. (**a**) The solution space for the fixed net weight constraint with two excitatory inputs is a line segment from $(0, \bar{J})$ to $(\bar{J}, 0)$ (a regular 1-simplex). (**b**) The solution space for the fixed net weight constraint with three excitatory inputs is an equilateral planar triangle (a regular 2-simplex). (**c**) Surface area of the regular $K-1$ simplex as a function of the number of presynaptic partners, K, for different net synaptic weights $\bar{J}$, with $p = 0$. (**d**) Relation between the in-degree that maximizes the simplex surface area, K^*, and the net synaptic weight, $(K^*)^p\bar{J}$. Solid lines: theoretical prediction. Dashed black lines: linear approximation.

The surface area of the simplex increases with the net excitatory weight, but for $\bar{J} \geq 1$ it has a maximum at positive K (Fig. 1c). The mode of this distribution gives the optimal degree (Methods 6.3):

$$(K^*)^p \bar{J} = (K^* + p - 1) \exp(-p) + \mathcal{O}(1/K^*) \tag{10}$$

revealing an approximately linear relationship, similar to the constraint on the maximum possible synaptic weight (Eq. 6). As for the bounded net weight, we can see from Eq. 10 that if $p = 1$, we obtain the condition $\bar{J} = 1/e$ (to leading order). So if $p = 1$ and $\bar{J} = 1/e$, the surface area is approximately independent of K. If $p = 1$ and $\bar{J} < 1/e$, the area decreases monotonically and vice versa.

2.4 Optimally flexible connectivity in Drosophila mushroom bodies

Testing these predictions requires joint measurements of neurons' total synaptic weight and number of synaptic partners. For this purpose we turned to dense electron micrographic (EM) reconstructions with synaptic resolution. Dense EM reconstructions have been published for the mushroom bodies of the first instar larval *D. melanogaster* [18] and the alpha lobe of the adult [50]. The reconstruction of the first instar larva includes all pre- and postsynaptic partners of the Kenyon cells (KCs). The adult's alpha lobe is defined by axons of KCs; that reconstruction does not include inputs onto the alpha lobe KCs' dendrites.

Since the fly EM data includes synapse counts but not synaptic weights, we assumed that the number of synapses, $\bar{S}$, is proportional to the physiologically constrained synaptic weight:

$$K^p \bar{J} = \alpha \bar{S} \tag{11}$$

where α is the constant relating the synapse count and the physiological weight. This assumes that the scaling with K^p arises from something other than the number of synapses. If it did arise from the number of synapses directly, then Eq. 11 would correspond to taking $p = 0$.

Our theory predicted (1) distributions of the numbers of synaptic partners proportional to the size of the space of allowed weights under a physiological constraint, and (2) an approximately linear relationship between the number of presynaptic partners to a neuron and its net weight (Eqs. 10, 6). As a first test, we asked how well these linear approximations described connectivity in the larval mushroom body by computing the Pearson correlation between K and $\bar{S}$. This corresponds to the more restricted hypothesis that connectivity exactly optimizes the size of these synaptic weight spaces. In the next section we will consider the more general hypothesis that these sizes serve as objective functions.

To measure excitatory connectivity, we excluded inputs from the inhibitory APL neuron and the modulatory dopaminergic, octopaminergic, and interneurons (but obtained similar results when including them). As in previous studies, we used only reliable multi-synapse connections (but obtained similar results when including single-synapse connections) [18, 50].

We began by examining neurons' input connectivity. Across all postsynaptic neurons in the first instar larval mushroom body, we saw an approximately linear relation between K and $\bar{S}$ ($r(K, \bar{S}) = 0.82$). We next examined whether this relationship depended on the postsynaptic cell type. We first examined the larval KCs, which had $r(K, \bar{S}) = 0.92$ (Fig. 4a). Their dendrites form claws around projection neuron axons, and these claws allow classification of the KCs by their maturity [18]. The youngest KCs have no claws, and the oldest a single claw. For young (clawless) KCs, we saw a near perfect linear relation (Fig. 4a black; $r(K, \bar{S}) = 0.99$). Clawed KCs were not explained as well by our theory (Fig. 4a; single-claw KCs in blue, $r(K, \bar{S}) = 0.67$, and multi-claw KCs in orange, $r(K, \bar{S}) = 0.77$).

In the alpha lobe of the adult mushroom body, we found a similarly linear relation between K and $\bar{S}$ to the larval mushroom body: $r(K, \bar{S}) = 0.82$ across all postsynaptic cells. For all KCs we found $r(K, \bar{S}) = 0.96$. The

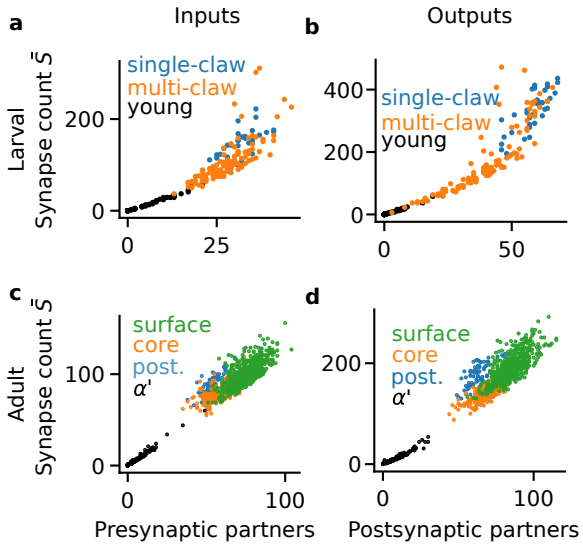

Fig 4. Relation between number of synaptic partners and synapse counts in *D. melanogaster* Kenyon cells. (**a**) Inputs to Kenyon cells (KCs) of the first instar larva. (**b**) Outputs of the first instar KCs. (**c**) Inputs to adult KCs in the α lobe. (**d**) Outputs of adult KCs in the α lobe.

Kenyon cells innervating the alpha prime lobe best matched our prediction (Fig. 4c black, $r(K, \bar{S}) = 0.99$). The KCs innervating the main alpha lobe are classified by the locations of their axons: posterior (Fig. 4c blue, $r(K, \bar{S}) = 0.69$), core (Fig. 4c orange, $r(K, \bar{S}) = 0.76$), and surface (Fig, 4c green, $r(K, \bar{S}) = 0.74$). Both those sets of results were similar when including inhibitory and modulatory inputs (r within 0.02).

We next turned to examine the output connectivity of Kenyon cells. Here, the simplex's surface area models a homeostatic regulation of the neuron's total output synaptic weight, while the simplex's volume models a bounded maximum output synaptic weight. We again examined reliable, multi-synapse connections but obtained similar results when including single-synapse connections. Similarly to the input connectivity for the larva, we found a high correlation between K and $\bar{S}$ across all Kenyon cells ($r(K, \bar{S}) = 0.93$), which was highest within the young KCs ($r(K, \bar{S}) = 0.99$; Fig. 4b, black). The single- and multi-claw KCs had $r)K, \bar{S} = 0.80$ and 0.86 respectively (Fig. 4b, blue and orange). In the adult, we found a high correlation between K and $\bar{S}$ across all Kenyon cells ($r(K, \bar{S}) = 0.930.95$), which was highest in the alpha prime Kenyon cells ($r(K, \bar{S}) = 0.97$). The alpha lobe Kenyon cells had $r(K, \bar{S}) = 0.92$ overall; the posterior, core, and surface Kenyon cells had $r(K, \bar{S})$ =0.69, 0.81, and 0.74 respectively.

The optimal configurations of connectivity for both the fixed and bounded net weight constraints were described by linear relationships between the total number of synapses and the number of synaptic partners, with slopes and intercepts determined by the two unknown parameters α and p. That prediction cannot determine which constraint better explains the connectivity data. Furthermore, that linear relationship would also be expected by simple random wiring models where the average number of synapses is the same across projections.

2.5 Flexible Kenyon cell input distributions

To distinguish between these possibilities, we return to the motivating idea that the size of the space of allowed weights for a given constraint should serve as an objective function for the circuit connectivity to maximize. If that constraint is our only information about circuit connectivity, it defines a distribution for the data where given a certain amount of synaptic weight $\bar{J}K^p$, the probability of observing a number of partners K is proportional to the size of the synaptic weight space it defines. For the fixed net weight constraint, for example, the predicted distribution of the data is proportional to the surface area of a simplex (Eq. 41). Similarly, for the bounded net weight constraint the predicted degree distribution is proportional to the volume under a simplex (Eq. 62). Each of these provided predictions for the distribution of degrees amongst KCs (Fig. 5a, b). We next asked which constraint best predicted connectivity in the drosophila mushroom bodies, and whether they provided better predictions than a simple random wiring model.

We examined the distributions of the numbers of presynaptic partners, K, across KCs (Fig. 6a). Since the dataset includes synapse counts rather than synaptic weights, we again assumed that synapse counts are proportional to the weight constraints with some unknown scale factor α (Eq. 11). We normalized the simplex volume and area, as functions of K, to obtain probability distributions (Methods, Eqs. 41, 62). These distributions take the net weight, $\alpha\bar{S}$, as a parameter. While $\bar{S}$ is measured for each neuron, α is unknown.

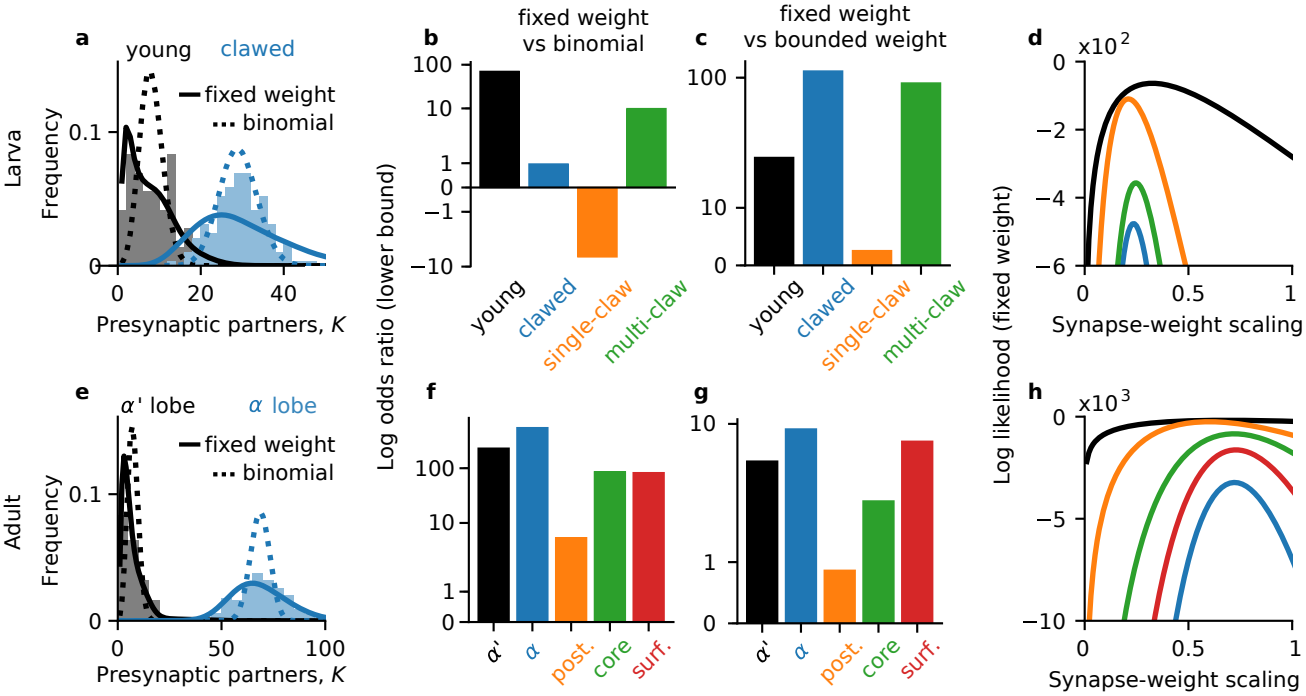

Fig 5. Kenyon cell input degree distributions. (**a**) Distribution of number of presynaptic partners for larval KCs. Shaded histograms: empirical distribution. Solid lines: the marginal simplex area distribution at the maximum likelihood value of α, after integrating out the number of synapses $\bar{S}$ against its empirical distribution. Dotted lines: the maximum likelihood binomial distribution using anatomical estimates for the potential partners (Methods:6.10). (**b**) Lower bound for the log posterior odds ratio for the fixed net weight and binomial wiring models. Positive numbers favor the fixed weight model. (**c**) Lower bound for the log posterior odds ratio for the fixed net weight and bounded net weight models; positive numbers favor the fixed weight model. (**d**) Log odds of the fixed net weight model as a function of the scaling between synapse counts and net synaptic weights. (**e-h**) Same as (**a-d**) but for adult alpha lobe KC axonal inputs.

To measure the performance of these models we computed their marginal likelihoods, integrating over all non-negative values of α in a Laplace approximation (Methods: 6.5). We first used flat priors for α. This allowed an analytic approximation of the posterior odds for the zero-truncated Poisson (simplex volume) model. The normalization constant for the simplex area distribution was not analytically tractable, so we found upper and lower bounds for it; these yield bounds for the posterior odds (Methods: 6.6, 6.7).

KC inputs from olfactory projection neurons also appear random, with little dependence on space or correlation between numbers of partners [7, 42]. Motivated by this, we also examined a simple random wiring model where $p_B(K|K > 0) \sim \text{Binomial}(N, q)$. As for the other models, we found the Laplace approximation for the zero-truncated binomial model and computed the posterior odds by marginalizing out the connection probability q (Methods: 6.11). We used anatomical measurements of the number of potential partners, N (Methods: 6.10).

In the larva, the simplex area model outperformed the binomial model for both young and clawed KCs (Fig. 5c, log odds ratio at least 70.46 and 0.97). We next asked how whether this depended on the number of claws, separately computing the marginal likelihood for KCs with each number of claws. The fixed net weight model outperformed the binomial wiring model for multi-claw KCs, but not single-claw KCs (Fig. 5c, log odds ratio at least 9.92 for multi-claw KCs; Fig. 8b, log odds at most -1.57 for single-claw KCs). Within multi-claw KCs, the binomial model also outperformed the fixed weight model for two-claw KCs, but not for KCs with at least three claws (Fig. 8b). We found similar results comparing the bounded net weight model with binomial wiring (Fig. 8c). The fixed net weight model outperformed the bounded weight model for all KC types (Fig. 5c). These results were similar when only examining KC-KC connectivity (Fig. 9a-d). Since single-claw KCs are younger than multi-claw KCs [18], these results suggest that flexibility under a homeostatically fixed net weight governs KC input connectivity early in development, with other factors shaping connectivity after sensory and behavioral experience.

It is possible that these results depend on the prior distribution for α. We used the naively uninformative flat prior. Since the distribution obtained from the simplex volume is a zero-truncated Poisson distribution, we also checked the Jeffreys prior for the Poisson distribution (Methods: 6.5) for α and q. We obtained similar results with this prior. The fixed net weight model outperformed the bounded weight model for all KC types with the Poisson Jeffreys prior also (Fig. 8a; log odds ratios of at least 1.34, 12.49, 1.37 and 9.86 for larval young, clawed, single- and multi-claw KCs respectively). The fixed net weight model and bounded net weight models outperformed the binomial model for young and multi-claw KCs (log odds at least 73.61 and 11.15 respectively), but not for single-claw or two-claw KCs (Fig. 8e, f; log odds at most -3.96 and -9.82 for single- and two-claw KCs).

We next asked whether how the relationship between anatomical and physiological synaptic weights exhibited a similar developmental trajectory, with multi-claw KCs appearing more similar to young KCs. To this end, we examined the likelihood of the data under the fixed net weight model as a function of the scaling parameter α (Fig. 5d). We saw that that the maximum likelihood value of α, $\hat{\alpha}$, decreased with KC age (maximum likelihood values of α: 0.33, 0.25, 0.21 for young, multi-claw and single-claw KCs, respectively). The scaling for single- and two-claw KCs were similar ($\hat{\alpha}$ of 0.2 for two-claw KCs), while KCs with three or more claws had $\hat{\alpha} \geq 0.25$. Under the simple model of Eq. 11, these suggest that the translation of synapse counts into a physiologically regulated net synaptic weight becomes weaker during KC maturation.

As in the larva, adult KCs exhibited a range of in-degrees. KCs in the alpha prime lobe receiving fewer axonal inputs than KCs in the alpha lobe (Fig. 5e). In the adult, the fixed net model explained the in-degree distribution of every KC type better than the binomial model (Fig. 5f; log odds at least 232.57, 551.5, 5.36, 85.82, and 83.02 for alpha prime, all alpha lobe, posterior, core and surface KCs respectively). The fixed net weight model also explained the in-degree distributions better than the bounded weight model (Fig. 5f; log odds at least 4.59, 9.0, 0.87, 2.0, and 6.96 for alpha prime, all alpha lobe, posterior, core and surface KCs respectively). The upper bounds for the log odds of the fixed net weight distribution were close to the lower bounds for the adult KCs (Fig. 10a, b). We found similar results using the Poisson Jeffreys prior for the unknown parameters α and q (Fig. 10d-f). In summary, the distributions of input degrees for KCs in the adult alpha prime and alpha lobes are best described by flexibility under a homeostatically fixed net synaptic weight.

The scaling between synapse counts and synaptic weights varied by KC type in the adult (Fig. 5h). The maximum likelihood values for α were $0.68, 0.6, 0.73, 0.72$ for alpha prime, posterior, surface and core KCs (ordered from approximately oldest to youngest). These suggest that in the alpha lobe, surface and core KCs have more input synaptic weight per synapse on average than posterior KCs. The log odds for the alpha prime KCs was much less sensitive to small values of α than the classes of alpha lobe KCs (Fig. 5h, black vs colored curves), suggesting a more heterogenous or flexible relationship between axonal input synapse counts and regulated synaptic weights in alpha prime KCs.

2.6 Flexible Kenyon cell output distributions

We next turned to examine the output connectivity of the larva Kenyon cells (Fig. 6a). Here, our predictions correspond to homeostatically fixed, or bounded, net output synaptic weights for KCs. As above, we compared these to a simple binomial random wiring null model.

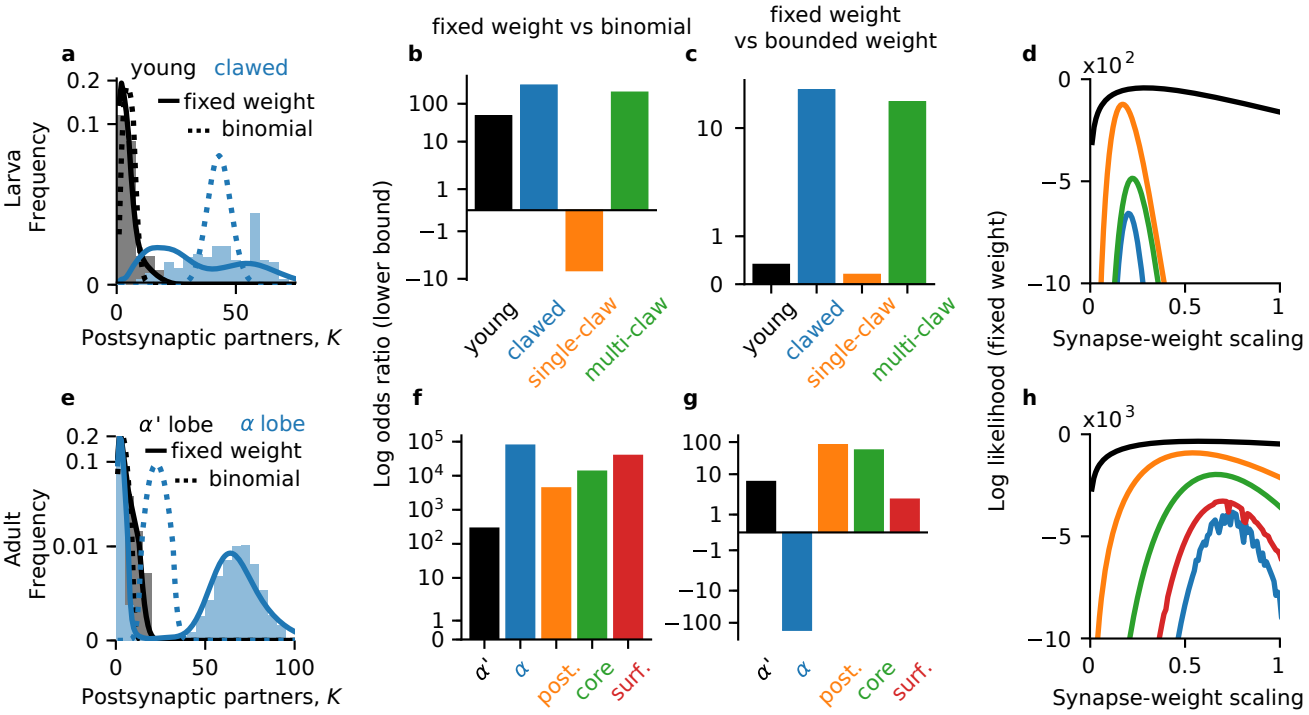

Fig 6. Kenyon cell output degree distributions. (**a**) Distribution of number of postsynaptic partners for larval KCs. Shaded histograms: empirical distribution. Solid lines: the marginal simplex area distribution at the maximum likelihood value of α, after integrating out the number of synapses $\bar{S}$ against its empirical distribution. Dotted lines: the maximum likelihood binomial distribution using anatomical estimates for the potential partners (Methods:6.10). (**b**) Lower bound for the log posterior odds ratio for the fixed net weight and binomial wiring models. Positive numbers favor the fixed weight model. (**c**) Lower bound for the log posterior odds ratio for the fixed net weight and bounded net weight models; positive numbers favor the fixed weight model. (**d**) Log odds of the fixed net weight model as a function of the scaling between synapse counts and net synaptic weights. (**e-h**) Same as (**a-d**) but for adult alpha lobe KC outputs.

Overall, we found similar results for the output connectivity degrees as for the inputs. For the larva KCs, the fixed net weight outperformed the binomial wiring for young and multi-claw KCs (log odds at least 48.17 and 201.8 respectively), but not for single- or two-claw KCs (log odds at most -0.78 and -0.50 respectively). For KCs with three or more claws, the log odds ratio for the fixed weight versus binomial wiring were at least 20.3 (Fig. 11b). The bounded net weight model outperformed the binomial wiring in the same cases - for young and clawed KCs, except for single- and two-claw KCs (Fig. 11c). The fixed net weight model described KC output degree distributions better than the bounded net weight for all types of KC in the larva (Fig. 6c, 11a). Under the Poisson Jeffreys prior, the only result that changed was that the bounded net weight was the best model for the young KC outputs (Fig. 11d-f). If we restrict the analysis to only KC-KC connectivity, then the fixed net weight model outperforms the binomial wiring and bounded net weight models for single-claw KCs (Fig. 9f, g), although not for two-claw KCs (not shown). Together, these results suggests that flexibility under a homeostatically fixed net synaptic weight regulates the input and output degree distributions of immature KCs, but that single- and two-claw KC degree distributions may be described better by a binomial wiring model.

We also examined how the likelihood of the data depended on the scaling between synapse counts and regulated synaptic weights for the outputs. As for the inputs, we found that the maximum likelihood values of α decreased with KC age, from 0.29 for young to 0.22 for multi-claw and 0.17 for single-claw KCs (Fig. 6d). The two-claw KCs exhibited a similar scaling as the single-claw KCs (0.17), while KCs with three or more claws had higher α values (0.24 for three- and four-claw KCs, 0.28 for five- and six-claw KCs). Similarly to for their inputs, these suggest that the relationship between net synapse counts and regulated net synaptic weights in the larva mushroom body may become weaker during KC maturation.

In the adult, Kenyon cells had heterogenous out-degrees, with alpha lobe KCs exhibiting a bimodal distribution (Fig. 6e). This bimodality was reflected in the out-degrees of posterior, core and surface KCs, rather than arising from one of those KC types (not shown). The fixed net weight models predicted adult KC out-degree distributions better than the binomial wiring model for all KC types (Fig. 6f), as did the bounded net weight model (Fig. 12f). The fixed net weight provided a better description for all the out-degree distributions of all types of adult KC than the bounded net weight, except when posterior core and surface KCs were all considered together (Fig. 6g). These results were consistent when using the Poisson Jeffreys prior for α and q (Fig. 12d-f). Together with the consistent results for adult KC input degrees (Fig. 5e-g), these suggest that flexibility under a fixed net synaptic weight governs KC connectivity in the alpha lobe of the mushroom body.

The scaling between the synapse count and net synaptic weight, α, exhibited similar patterns for adult KC outputs as for their inputs (Fig. 6h vs Fig. 5h). The maximum likelihood values of α were 0.58, 0.54, 0.7 and 0.67 for alpha prime, posterior, surface and core KCs respectively (in approximate developmental order). These suggest a divide with more mature KCs having more synaptic weight per synapse, on average, than younger KCs. The log odds for the alpha prime KCs was also much less sensitive to low values of α than the other KC types (Fig. 6h black vs colored curves), suggesting a more heterogenous or flexible relationship between axonal input synapse counts and regulated output synaptic weights similar to for the input synaptic weights (Fig. 5h black vs colored curves).

3 Discussion

In simple neural network models, constraints define a space of possible synaptic weights (the "constraint space"; Fig. 1a, b gray regions), while the synaptic weights that perform a particular computation define another space (the "computation space"; Fig. 1a, b colored regions). The intersection of the constraint and computation spaces defines the allowed synaptic weights (the "solution space"). The size of the solution space is then bounded by the size of the constraint space and the size of the computation space. A large solution space can be beneficial to maintain performance if synaptic weights fluctuate, or to enable fast learning. While the computation space is circuit-dependent and may change with experience and environment, the constraint space reflects the underlying neurophysiology. Maximizing its size may prevent the constraints from interfering with task-specific learning. On the other hand, this may also introduce a non-trivial relationship between the dimensionality of possible computations and the constraint space. Organisms may need to coadapt the physiological constraints and the dimensionality of the input space to match the problems that they are required to solve. It is an open problem whether and how these two constraints interact.

Many studies have examined the hypothesis that neural circuits might be optimal for sensory inference, metabolically efficient encoding, or associative learning and memory (e.g., [1–3, 5, 8, 9, 15, 35, 40]). Minimizing the amount of wire used to connect neural circuits can predict the spatial layout of neural systems (e.g., [6, 10, 11, 17, 60]) and dendritic arborizations [13, 14]. We examined, in contrast, the idea that the number of synaptic partners to a neuron might be structured to make constraints flexible: to allow many different connectivity configurations. In the models discussed here (Eqs. 7, 5), metabolic constraints or wiring constraints could be thought of as fixing the total available synaptic weight (the parameter $\bar{J}$).

This hypothesized optimization implies a distribution of connectivity degrees: a probability that, given a certain total synaptic weight, a neuron receives (or sends) input to K partners. We elucidated the optimally flexible numbers of synaptic partners for a neuron and how these depended on the scaling of synaptic weights. We tested these predictions in *D. melanogaster* mushroom bodies, using a complete wiring diagram for the larval Kenyon cells (KCs) [18] and a wiring diagram for connectivity within the alpha lobe of the adult [50]. (The alpha lobe is defined by the axons of KCs, so those data do not include dendrites.) Random wiring of KCs [7, 42] has been discussed as a mechanism to facilitate associative learning [34, 38], focusing on apparent lack of structure in glomerular projections to KCs. This notion of random wiring begs the question: what principle governs the distribution of that random process? Our work tests a hypothesis for that principle: flexibility under constraints.

We found that in the larva, the degree distributions of immature KCs (clawless and multi-clawed KCs) were best explained by flexibility under a homeostatically fixed net weight, compared to a bounded net weight or a binomial random wiring model (Fig. 5b, c). The mature KCs (single- and two-claw) were, in contrast, best explained by a binomial wiring model (Fig. 5b, c orange; Fig. 8b, c; Fig. 11b, c). This was the case for inputs to KCs (Figs. 5, 8) and outputs from them (Figs. 6, 11). These suggest a developmental process in the larva governing the distribution of KC connectivity degrees.

In the adult KCs, flexibility under a homeostatically fixed net weight provided the best explanation for axonal connectivity of all KC types in the alpha prime and alpha lobe (Figs. 5f, g; 6f, g) except when lumping together the outputs of all alpha lobe KCs; then flexibility under a bounded net weight provided the best prediction (Fig. 6f, g). The adult connectivity data does not include dendritic KC inputs, so we also examined axonal connectivity in the larva with similar results (Fig. 9). Together with the larva results, these suggest that KCs undergo synaptic scaling of their input and output synapses. There is evidence for homeostatic regulation of inputs elsewhere in the *D. melanogaster* nervous system. Blocking acetylcholine (ACh) in drosophila motor neurons leads to a homeostatic increase in the strength of newly transcribed ACh receptors, with a concomitant homeostatic increase in A-type K+ channels [43]. Manipulation of the total input to the aCC neuron elicits compensatory changes to its dendritic tree [51]. In the adult *D. melanogaster*, KC-MBON projections can undergo bidirectional plasticity [12, 27], required for synaptic scaling.

3.1 Measuring synaptic weight spaces

We derived theoretical predictions for the relationship between the net or maximal synaptic weight, $\bar{J}$, and the number of synaptic partners of a neuron, K. These predictions derived from considering the size of the space of synaptic weights satisfying that constraint, as the number of synaptic partners varied. If the weights were measured in physical units, the surface areas or volumes we considered would have different units for different values of K. To compare them, we nondimensionalized the weights, dividing them by the size of a measurable change in the synaptic weights, ΔJ. If ΔJ is small compared to the total available synaptic weight, the number of noticeably different synaptic weight vectors satisfying the bounded net weight is then proportional to the volume under a simplex (and similar for the homeostatically fixed net weight and the surface area). Due to the nondimensionalization, these sizes can also be thought of as relative to the volume of a hypercube of measurable synaptic weight units $(\Delta J)^K$.

In measuring the spaces of synaptic weights, we also assumed that the synaptic weight configuration can travel in a straight line between any two configurations, so that distances in the space of synaptic weights are Euclidean, measured by the root mean squared difference of their coordinates. If synaptic weights could not travel in a straight line, but rather each synapse would have to be potentiated or depressed separately, then we should instead use the 1-norm given by the sum of absolute differences. This changes the measure of the surface area of the simplex, replacing $\sqrt{K}$ by K in Eq. 7. This does not change the results of our analysis of KC input connectivity (Figs. 13, 14). For KC output connectivity, the bounded net weight was a better model than the fixed net weight, under the 1-norm for weight changes, for larval young KCs (Fig. 15) and adult surface KCs (Fig. 16).

Synaptic weights in our theory correspond to the variable regulated by homeostatic or resource constraints, while the data we examined were synapse counts. We assumed a simple relation between synapse counts and the synaptic weights for fly mushroom body synapses (Eq. 11) but this relationship must actually depend on the physiology and biochemistry underlying the homeostatic regulation or resource constraints. Taking into account the distance from a synapse to spike initiation zones and active dendritic conductances, could allow more accurate measurements of the physiological synaptic weight [46]. Synaptic weights may also vary discretely, with a relatively small number of units available N [45]. In combination with homeostatic or resource constraints, this implies a restricted combinatorial composition of the net synaptic weight from individual connections' contributions. The geometric formulation here is then a poor approximation to the number of allowed configurations.

3.2 Flexible connectivity and circuit development

It is interesting to consider these results in the context of development. Computational flexibility should be desirable for an organism's fitness, allowing the organism to solve problems in a variety of environments. One mechanism of adaptability and flexibility is to build the nervous system out of computationally flexible units, that may over time adapt to specific computational roles. Our results are suggestive that this type of strategy may be at play in the development of mushroom body connectivity in the first instar *D. melanogaster* larva. Figures 8 and 11 show that the log odds for young larval Kenyon cells vastly favor the constraints models over the binomial model. The odds also approximately decreasingly favor the constraint model with age (single clawed cells tend to be older than multi-clawed cells [18]). One can see this in Figures 4a, b, as the young larval Kenyon cells show a more linear relationship as predicted by our theory. Our results suggest that Kenyon cell connectivity might be optimally flexible early in development, developing specific function as the organism matures.

Kenyon cell location also reflects development in the adult Drosophila mushroom body alpha lobe, with alpha prime KCs born before alpha lobe KCs [36] and within the alpha lobe, core KCs born later than surface KCs [37]. We found that flexible connectivity under constraints on the net synaptic weight outperformed the binomial random wiring model most for the alpha prime KCs, and more for core than surface KCs (Figs. 5f, 6f, 10, 12). These suggest that flexibility under constraints might also reflect a developmental or experience-dependent progression in the alpha lobe KCs, but it remains a better explanation for their connectivity than binomial wiring even in the more mature KCs of the adult.

4 Acknowledgments

We thank Ramakrishnan Iyer and Casey Schneider-Mizell for helpful discussions. We wish to thank the Allen Institute founder, Paul G. Allen, for his vision, encouragement and support.

5 Author contributions

Conceptualization: G.K.O and M.A.B. Formal analysis: G.K.O. Writing (original draft): G.K.O. Writing (review and editing): G.K.O and M.A.B. Supervision: M.A.B.

6 Methods: Size of the synaptic weight constraint space

6.1 Measuring synaptic weight configurations

First, consider measuring the available configurations of synaptic weights when they can vary continuously. Consider the total synaptic weight, divided into K segments (Fig. 7). For one synaptic weight, the measure of the weight configurations is

$$\int_0^{\bar{J}} dJ_1 = \bar{J} \tag{12}$$

For two synaptic weights, the available configurations are measured by

$$\int_0^{\bar{J}} \int_{J_1}^{\bar{J}} dJ_2 \, dJ_1 = \frac{\bar{J}^2}{2} \tag{13}$$

and in general,

$$\int_0^{\bar{J}} \int_{J_1}^{\bar{J}} \int_{J_2}^{\bar{J}} \cdots \int_{J_{K-1}}^{\bar{J}} dJ_K \cdots dJ_3 \, dJ_2 \, dJ_1 = \frac{\bar{J}^K}{K!} \tag{14}$$

which is the volume under the simplex with vertex length $\bar{J}$.

Now consider synaptic weights that vary discretely by ΔJ, with $\bar{J} = N\Delta J$. How many ways can we assign N units of synaptic weight amongst K partners? For $K = 1$, this is N. For two synapses, this is

$$\sum_{n_1=1}^{N} \sum_{n_2=n_1}^{N} = \frac{N(N-1)}{2} \tag{15}$$

and in general the number of combinations of N units of synaptic weight in K connections is given by the binomial coefficient

$$\binom{N}{K} = \frac{N!}{K!\,(N-K)!} \tag{16}$$

For large N, the binomial coefficient is

$$\frac{N^K}{K!} \left(1 + \mathrm{O}\left(1/N\right)\right) \tag{17}$$

which approximates the answer of continuous weights above.

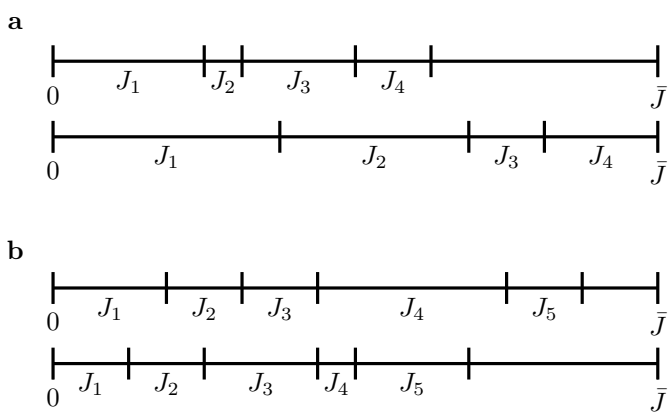

Fig 7. Synaptic weight configurations. a) Two example configurations of $K = 4$ synaptic weights with $J_1 + J_2 + J_3 + J_4 \leq \bar{J}$. **b)** Two examples of $K = 5$ synaptic weights with sum bounded by $\bar{J}$.

6.2 Neural resource constraints

Here we derive the volume of the constraint space for the synaptic weights for a neuron receiving K inputs. For generality, we allow the sum of synaptic weights to scale as K^p. If $\sum_j J_j \leq \bar{J}K^p$ then the weights live under the $(K-1)$-simplex with volume

$$V = \frac{(\bar{J}K^p)^K}{K!} \tag{18}$$

The volume is non-decreasing in $\bar{J}$. We compute the derivative of the surface area with respect to K by analytically continuing the factorial as the Gamma function, yielding

$$\begin{aligned}\frac{\partial V}{\partial K} &= \frac{(\bar{J}K^p)^K}{K!}\left(\ln \bar{J}K^p + p + \gamma - H_K\right) \\ &\approx \frac{(\bar{J}K^p)^K}{K!}\left(\ln \bar{J}K^p + p - \ln K - \frac{1}{2K} + \mathcal{O}\left(K^{-2}\right)\right)\end{aligned} \tag{19}$$

where H_X is the Xth harmonic number,

$$H_X = \sum_{x=1}^{X} \frac{1}{x} \tag{20}$$

We used Euler's expansion for the harmonic numbers,

$$H_X = \gamma + \ln X + \frac{1}{2X} + \mathcal{O}\left(X^{-2}\right) \tag{21}$$

At a critical point in K, truncating $\mathcal{O}(1/K^2)$ and higher-order terms, we find

$$\bar{J} \approx e^{\frac{1}{2K^*} - p}(K^*)^{1-p} \tag{22}$$

Alternatively, the critical point can be calculated without first extending K to real numbers by using ratios:

$$1 = \frac{V(K^*)}{V(K^*+1)} = \frac{(K^*+1)^{1-p}}{\bar{J}}\left(\frac{K^*}{K^*+1}\right)^{pK^*} \tag{23}$$

which yields

$$\bar{J}(K^*)^p = (K^*+1)\left(\frac{K^*}{K^*+1}\right)^{p(K^*+1)} = \exp(-p)\left(K^*+1-p\right) + \mathcal{O}(1/K^*) \tag{24}$$

6.3 Fixed total postsynaptic weight

If $\sum_j J_j = \bar{J}K^p$ then we have the surface area of the $K-1$ simplex. We consider a regular simplex (equal side lengths) with vertex length $\bar{J}K^p$ (from the origin to any vertex). Its surface area is

$$A = \frac{(\bar{J}K^p)^{K-1}\sqrt{K}}{(K-1)!} \tag{25}$$

which can be computed by varying the volume (Section 6.2) along the normal vector from the origin to the center of the simplex's outermost face, $\vec{j} = \frac{\bar{J}}{K}\vec{1}$. This can be computed by differentiating with respect to the edge length and scaling by the length of the normal vector. By the same method as above, the derivative with respect to K is

$$\begin{aligned}\frac{\partial A}{\partial K} &= \frac{(\bar{J}K^p)^{K-1}}{2\sqrt{K}(K-1)!}\left(2K\ln(\bar{J}K^p) + 2(K-1)p - 2K(H_{K-1} - \gamma) + 1\right) \\ &\approx \frac{(\bar{J}K^p)^{K-1}}{2\sqrt{K}(K-1)!}\left(2K\ln(\bar{J}K^p) + 2(K-1)p - 2K\left(\ln(K-1) + \frac{1}{2(K-1)} + \mathcal{O}\left(\frac{1}{K^2}\right)\right) + 1\right)\end{aligned} \tag{26}$$

Since H_{K-1} appears in the derivative, we only consider the derivative at $K \geq 2$. At a critical point in K, truncating $\mathcal{O}(1/K^2)$ and higher-order terms yields

$$\begin{aligned}
\ln \bar{J} &\approx \frac{1}{2K(K-1)} \left(-2p(K-1)^2 + 2K(K-1)\left(\ln(K-1) - p\ln K\right) + 1\right) \\
&= \frac{1}{2K}\left(-2p(K-1) + 2K\left(\ln(K-1) - p\ln K\right)\right) + \frac{1}{2K(K-1)} \\
&= \ln(K-1) - p\left(\ln K + \frac{K-1}{K}\right) + \frac{1}{2K(K-1)} \\
\bar{J} &\approx K^{-p}(K-1)\exp\left(\frac{1}{2K(K-1)} - p\frac{K-1}{K}\right)
\end{aligned} \tag{27}$$

If we do not continue to real K first, we instead have

$$1 = \frac{A(K^*)}{A(K^*+1)} = \frac{(K^*)^{1-p}}{\bar{J}}\left(\frac{K^*}{K^*+1}\right)^{pK^*+\frac{1}{2}} \tag{28}$$

which yields

$$\bar{J}(K^*)^p = K^*\left(\frac{K^*}{K^*+1}\right)^{pK^*+\frac{1}{2}} = \left(K^* + \frac{p-1}{2}\right)\exp(-p) + \mathcal{O}(1/K^*) \tag{29}$$

6.4 Fixed net weight with separate changes in individual synaptic weights

Above we assumed that synaptic weight configurations could travel between different points in the synaptic weight space along straight lines, endowing the synaptic weight space with a Euclidean norm. This amounts to assuming that synaptic weights can vary together. This could be interpreted, for example, as the allowing a unit of synaptic weight (a receptor, perhaps) to be transferred directly between synapses. An alternative is to assume that synaptic weights must move separately, which corresponds endowing the synaptic weight space with the 1-norm. In the above interpretation this would mean separating the removal of a receptor from one synapse from the addition of a receptor to another synapse.

This changes the surface area of the simplex, since the length of that normal vector is now K instead of $\sqrt{K}$:

$$A_1 = \frac{(\bar{J}K^p)^{K-1}K}{(K-1)!} \tag{30}$$

and its derivative with respect to K is (to order $1/K$):

$$\frac{\partial A_1}{\partial K} \approx \frac{(\bar{J}K^p)^{K-1}}{(K-1)!}\left(K\ln\bar{J}K^p + (K-1)p - K\left(\ln(K-1) + \frac{1}{2(K-1)} + \mathcal{O}\left(\frac{1}{K^2}\right)\right) + 1\right) \tag{31}$$

At a critical point in K, truncating $\mathcal{O}(1/K^2)$ and higher-order terms yields

$$\bar{J} \approx K^{-p}(K-1)\exp\left(\frac{1}{K(K-1)} - p\frac{K-1}{K}\right) \tag{32}$$

Alternatively, from the requirement

$$1 = \frac{A(K^*)}{A(K^*+1)} \tag{33}$$

we obtain

$$\bar{J}(K^*)^p = \exp(-p)\left(K^* + \frac{p}{2} - 1\right) + \mathcal{O}(1/K^*) \tag{34}$$

6.5 Model comparison

Under equal prior likelihoods for two models X and Y, the posterior odds ratio between two models, X and Y is

$$\frac{p_X(K_i|\bar{S}_i)}{p_Y(K_i|\bar{S}_i)} = \frac{\int d\alpha \ \prod_i p_X(K_i|\bar{S}_i,\alpha)p(\alpha)}{\int d\alpha \ \prod_i p_Y(K_i|\bar{S}_i,\alpha)p(\alpha)} \tag{35}$$

where i indexes data points. We consider the Laplace approximations for the posterior odds, obtained by expanding the log likelihood in α around the maximum likelihood value,

$$\hat{\alpha} = \arg\max_{\alpha} \prod_i p_X(K_i|\bar{S}_i,\alpha) \tag{36}$$

The Laplace approximation yields:

$$\begin{aligned}\int d\alpha \ p(\alpha) \prod_i \ p_X(K_i|\bar{S}_i,\alpha) &= \int d\alpha \ p(\alpha) \prod_i \ \exp \ln p_X(K_i|\bar{S}_i,\alpha) \\ &\approx \int d\alpha \ p(\alpha) \prod_i \ p_X(K_i|\bar{S}_i,\hat{\alpha}) \exp \frac{-(\alpha-\hat{\alpha})^2}{2\sigma_i^2}\end{aligned} \tag{37}$$

where the integrals run over the allowed range for α and

$$\sigma_i^2 = -\left.\frac{\partial^2}{\partial\alpha^2} \ln p_X(K_i|\bar{S}_i,\alpha)\right|_{\hat{\alpha}} \tag{38}$$

Under a flat prior for non-negative α, the marginal likelihood is:

$$p_X(K_i|\bar{S}_i) \approx \left(\prod_i p_X(K_i|\bar{S}_i,\hat{\alpha})\right) \sqrt{\frac{\pi\sigma^2}{2}} \left(1 + \mathrm{Erf}\left(\frac{\hat{\alpha}}{\sqrt{2\sigma^2}}\right)\right) \tag{39}$$

where $1/\sigma^2 = \sum_i 1/\sigma_i^2$. The simplex volume distribution is a truncated Poisson; we might reasonably use the Jeffreys prior for the Poisson distribution, $p(\alpha) \propto 1/\sqrt{\alpha}$. In that case, the marginal likelihood is

$$p_X(K_i|\bar{S}_i) \approx \left(\prod_i p_X(K_i|\bar{S}_i,\hat{\alpha})\right) \frac{\pi\sqrt{\hat{\alpha}}}{2} \exp\left(-\frac{\hat{\alpha}^2}{4\sigma^2}\right) \left(\mathcal{I}_{-\frac{1}{4}}\left(\frac{\hat{\alpha}^2}{4\sigma^2}\right) + \mathcal{I}_{\frac{1}{4}}\left(\frac{\hat{\alpha}^2}{4\sigma^2}\right)\right) \tag{40}$$

where $\mathcal{I}_a$ is the modified Bessel function of the first kind. We will drop the indices on $K, \bar{S}$ in most of the remaining sections, reintroducing themwhere necessary.

6.6 Laplace approximation for simplex area distribution

The simplex area distribution is

$$p_A(K|\bar{S},p) = \frac{1}{Z_A(\bar{S},\alpha)} \frac{(\alpha\bar{S})^{K-1}\sqrt{K}}{(K-1)!} \tag{41}$$

where

$$Z_A(\bar{S},\alpha) = \sum_{K=1}^{\infty} \frac{(\alpha\bar{S})^{K-1}\sqrt{K}}{(K-1)!} \tag{42}$$

To calculate $\hat{\alpha}$ and σ^2 we need the derivatives of $\ln p_A$.

$$\frac{\partial}{\partial\alpha} \ln p_A = \frac{\partial}{\partial\alpha} \ln A - \frac{\partial}{\partial\alpha} \ln Z \tag{43}$$

where

$$\frac{\partial}{\partial\alpha}\ln A = \frac{K-1}{\alpha} \tag{44}$$

and

$$\frac{\partial}{\partial\alpha}\ln Z = \frac{\frac{\partial}{\partial\alpha}Z}{Z} \tag{45}$$

We next approximate $\frac{\partial}{\partial\alpha}Z$.

$$\begin{aligned}\frac{\partial}{\partial\alpha}Z &= \sum_{K=2}^{\infty}\frac{(\alpha\bar{S})^{K-2}}{(K-2)!}\sqrt{K}S \\ &= S\sum_{K=1}^{\infty}\frac{(\alpha\bar{S})^{K-1}}{(K-1)!}\sqrt{K+1} \\ &= S\sum_{K=1}^{\infty}\frac{(\alpha\bar{S})^{K-1}}{(K-1)!}\sqrt{K}\sqrt{1+\frac{1}{K}} \\ &\approx SZ\end{aligned} \tag{46}$$

How good is that approximation? For $K \geq 1$, $\sqrt{1+1/K}$ is bounded above by $\sqrt{2}$ and below by 1. So,

$$SZ < \frac{\partial}{\partial\alpha}Z < \sqrt{2}SZ \tag{47}$$

Inserting these into the critical point equation for $\hat{\alpha}$ provides the bounds:

$$\frac{\sum_i(K_i-1)}{\sqrt{2}\sum_i\bar{S}_i} < \hat{\alpha} < \frac{\sum_i(K_i-1)}{\sum_i\bar{S}_i} \tag{48}$$

We will also need the curvature of $\ln p_A$ w.r.t. α at $\hat{\alpha}$:

$$\sigma^2 = -\frac{\partial^2}{\partial\alpha^2}\ln p_A \tag{49}$$

Similarly to the first derivative,

$$\frac{\partial^2}{\partial\alpha^2}\ln p_A = \frac{\partial^2}{\partial\alpha^2}\ln A - \frac{\partial^2}{\partial\alpha^2}\ln Z \tag{50}$$

where

$$\frac{\partial^2}{\partial\alpha^2}\ln A(K|\bar{S},\alpha) = -\frac{(K-1)}{\alpha^2} \tag{51}$$

We use the identity

$$\frac{\partial^2}{\partial\alpha^2}\ln Z = \frac{\frac{\partial^2}{\partial\alpha^2}Z}{Z} - \frac{\left(\frac{\partial}{\partial\alpha}Z\right)^2}{Z^2} \tag{52}$$

The curvature of Z is

$$\begin{aligned}\frac{\partial^2}{\partial\alpha^2}Z &= S^2\sum_{K=3}^{\infty}\frac{(\alpha\bar{S})^{K-3}}{(K-3)!}\sqrt{K} \\ &= S^2\sum_{K=1}^{\infty}\frac{(\alpha\bar{S})^{K-1}}{(K-1)!}\sqrt{K+2} \\ &= S^2\sum_{K=1}^{\infty}\frac{(\alpha\bar{S})^{K-1}}{(K-1)!}\sqrt{K}\sqrt{1+\frac{2}{K}} \\ &\approx S^2Z\end{aligned} \tag{53}$$

The final term $\sqrt{1+\frac{2}{K}}$ is bounded above by $\sqrt{3}$ and below by 1, so

$$S^2 Z < \frac{\partial^2}{\partial\alpha^2} Z < \sqrt{3} S^2 Z \tag{54}$$

Defining upper and lower bounds for $\frac{\partial^2}{\partial\alpha^2}\ln Z$ using the upper and lower bounds of the first and second terms in Eq. 52 yields:

$$-S^2 < \frac{\partial^2}{\partial\alpha^2}\ln Z < (\sqrt{3}-1)S^2 \tag{55}$$

The upper bound for $\frac{\partial^2}{\partial\alpha^2}\ln Z$ provides an upper bound for σ^2, while neglecting Z provides a lower bound for σ^2 (since $Z \geq 1$ from Eq. 42, so that $\ln Z \geq 0$):

$$\frac{K-1}{\alpha^2} \leq \sigma^2 < \frac{K-1}{\alpha^2} + (\sqrt{3}-1)S^2 \tag{56}$$

The posterior odds for the simplex area are:

$$\int d\alpha\, p(\alpha) \prod_i p_A(K_i|\bar{S}_i,\alpha) \approx \left(\prod_i p_A(K_i|\bar{S}_i,\hat{\alpha})\right) \int d\alpha\, p(\alpha) \exp\left(\frac{(\alpha-\hat{\alpha})^2}{2\sigma^2}\right) \tag{57}$$

where $\sigma^2 = 1/\sum_i 1/\sigma_i^2$. We use the upper and lower bounds for σ_i^2 to define upper and lower bounds, respectively, for the likelihood's variance:

$$\begin{aligned} \sigma_U^2 &= \left(\sum_i \left(\frac{(K_i-1)}{\hat{\alpha}^2} + \left(\sqrt{3}-1\right)\bar{S}_i^2\right)^{-1}\right)^{-1} \\ \sigma_L^2 &= \left(\sum_i \left(\frac{(K_i-1)}{\hat{\alpha}^2}\right)^{-1}\right)^{-1} \end{aligned} \tag{58}$$

We compute $\hat{\alpha}$ numerically by maximizing the likelihood, and compute $p_A(K_i|\bar{S}_i,\hat{\alpha})$ also numerically, estimating Z by ranging over $K = 1$ to $2\max_i \bar{S}_i$.

6.7 Bounds for the posterior odds of the simplex area distribution

The derivative of the posterior odds under the flat prior, Eq. 39, with respect to σ is proportional to

$$1 - \frac{\sqrt{2}\alpha \exp\left(-\frac{\alpha^2}{2\sigma^2}\right)}{\sqrt{\pi}s} + \mathrm{Erf}\left(\frac{\alpha}{\sqrt{2}\sigma}\right) \tag{59}$$

Since $\alpha > 0$ and $\sigma > 0$, the last term is bounded between 0 and 1. The middle term is of the form $x\exp(-x^2/2)$, which is maximized by $1/\sqrt{e}$ at $x = 1$. Since $\sqrt{2/\pi e} < 1$, the middle term is less than 1 and the derivative of the posterior odds under a flat prior for α, with respect to σ^2, is non-negative. The upper bound for σ^2 thus provides an upper bound on the posterior odds. We see that the posterior likelihood $\prod_i p_A(K_i|\bar{S}_i)$ increases from σ_L^2 to σ_U^2 (reflected in the log posterior odds ratio for the simplex volume vs the simplex area, Figs. 8-12a, b).

The derivative of the posterior odds under the Poisson Jeffreys prior, Eq. 40, with respect to σ^2, is proportional to

$$-\frac{\alpha^2}{2\sigma^3}\exp\left(-\frac{\alpha^2}{4\sigma^2}\right)\left(\mathcal{I}_{-\frac{5}{4}}\left(\frac{\alpha^2}{4\sigma^2}\right) + \mathcal{I}_{-\frac{3}{4}}\left(\frac{\alpha^2}{4\sigma^2}\right) + 2\mathcal{I}_{-\frac{1}{4}}\left(\frac{\alpha^2}{4\sigma^2}\right) + 2\mathcal{I}_{\frac{1}{4}}\left(\frac{\alpha^2}{4\sigma^2}\right) + \mathcal{I}_{\frac{3}{4}}\left(\frac{\alpha^2}{4\sigma^2}\right) + \mathcal{I}_{\frac{5}{4}}\left(\frac{\alpha^2}{4\sigma^2}\right)\right) \tag{60}$$

We saw that the posterior odds for the simplex area distribution also increased with σ^2 for the Poisson Jeffreys prior (Figs. 8-12d, e).

6.8 Laplace approximation for the simplex area under the 1-norm for synaptic weights

Changing the norm for the synaptic weights leaves the derivation of the posterior odds mostly unchanged. The factors of $\sqrt{K}$ in the normalization constant are replaced by K; this removes the square roots in the derivation of the upper bound for the variance with respect to α so that

$$\frac{K-1}{\alpha^2} \leq \sigma^2 < \frac{K-1}{\alpha^2} + 2S^2 \tag{61}$$

6.9 Laplace approximation for simplex volume distribution

The simplex volume distribution is:

$$p_V(K|\bar{S}, p) = \frac{(\alpha\bar{S})^K}{Z_V(\bar{S}, \alpha)K!} \tag{62}$$

The normalization constant Z is

$$Z_V(\bar{S}, \alpha) = \sum_{K=1}^{\infty} \frac{(\alpha\bar{S})^K}{K!} = \exp\left(\alpha\bar{S}\right) - 1 \tag{63}$$

so the simplex volume distribution is a zero-truncated Poisson distribution. Similarly to for the simplex area, we will make a Laplace approximation for the simplex volume distribution around $\hat{\alpha}$, leading to the posterior odds Eq. 39 (for a flat prior on non-negative α) or Eq. 40 (for the Poisson Jeffreys prior). To calculate the Laplace approximation for the posterior odds we need $\hat{\alpha}$ and σ^2. The derivatives of $\ln p_V$ can be calculated directly; again dropping indices over measurements,

$$\begin{aligned} \frac{\partial}{\partial\alpha} \ln p_V(K|\bar{S}, \alpha) &= \frac{K}{\alpha} + \bar{S}\left(\frac{1}{1-\exp\alpha\bar{S}} - 1\right) \\ \frac{\partial^2}{\partial\alpha^2} \ln p_V(K|\bar{S}, \alpha) &= -\frac{K}{\alpha^2} + \left(\frac{\bar{S}}{2}\operatorname{Csch}\left(\frac{\alpha\bar{S}}{2}\right)\right)^2 \end{aligned} \tag{64}$$

So we have

$$\sigma^2 = \left(\sum_i \left(\frac{K_i}{\hat{\alpha}^2} - \left(\frac{\bar{S}_i}{2}\operatorname{Csch}\left(\frac{\hat{\alpha}\bar{S}_i}{2}\right)\right)^2\right)^{-1}\right)^{-1} \tag{65}$$

and the maximum likelihood solution for α satisfies

$$0 = \sum_i \frac{K_i}{\hat{\alpha}} - \frac{\bar{S}_i}{1-\exp\hat{\alpha}\bar{S}_i} \tag{66}$$

6.10 Zero-truncated binomial model

We consider a model where the number of synaptic partners, given that there is at least one, is $K \sim \text{Binomial}(N, p)$. We used the zero-truncated binomial distribution for a fair comparison with the simplex area and volume distributions, which are not defined for $K = 0$:

$$p_B(K_i|N, q) = \binom{N}{K_i} \frac{q^{K_i}(1-q)^{N-K_i}}{1-(1-q)^N} \tag{67}$$

(q is the success probability). For connections to larval KCs, we used the total number of traced projection neurons (PNs) and KCs as the binomial parameter N, averaged over the two sides of the brain [18]. For projections from larval KCs, we used the total number of KCs and output neurons, averaged over the two sides, as N. For projection to adult KCs, we used the number of Kenyon cells plus 150 (the estimated number of

olfactory PNs) as N [29]. For projections from adult KCs, we used the number of KCs and output neurons labelled in the data as N. Our results were not sensitive to varying N.

6.11 Laplace approximation for zero-truncated binomial model

The marginal likelihood for the zero-truncated binomial with distribution p_B is

$$p_B(\{K_i\}) = \int dq\, p(q) \prod_i p_B(K_i|N,q) \approx \left(\prod_i p_B(K_i|N,\hat{q})\right) \int dq\, p(q) \prod_i \exp\left(-\frac{(q-\hat{q})^2}{2\sigma^2}\right) \tag{68}$$

The derivates of $\ln p_B$ are, again dropping indices on K,

$$\begin{aligned} \frac{\partial}{\partial q} \ln p_B &= \frac{K}{q} - \frac{N-K}{1-q} - \frac{N(1-q)^{N-1}}{1-(1-q)^N} \\ \frac{\partial^2}{\partial q^2} \ln p_B &= -\frac{K}{q^2} + \frac{N-K}{(1-q)^2} + \frac{N\left(N-1+(1-q)^N\right)(1-q)^{N-2}}{\left((1-q)^N-1\right)^2} \end{aligned} \tag{69}$$

The maximum likelihood parameter $\hat{q}$ for the zero-truncated binomial, with M samples of K, each with N trials, obeys:

$$\frac{\hat{q}}{1-(1-\hat{q})^N} = \frac{\sum_{i=1}^M K_i}{MN} \tag{70}$$

and the variance at $\hat{q}$ is

$$\sigma^2 = \left(\sum_i \left(\frac{K_i}{\hat{q}^2} - \frac{N-K_i}{(1-\hat{q})^2} - \frac{N\left(N-1+(1-\hat{q})^N\right)(1-\hat{q})^{N-2}}{\left((1-\hat{q})^N-1\right)^2}\right)^{-1}\right)^{-1} \tag{71}$$

7 Data Availability

The mushroom body connectivity data are available from the relevant publications [18, 50].

References

1. J. S. Albus. A theory of cerebellar function. *Mathematical Biosciences*, 10(1):25–61, Feb. 1971.

2. J. J. Atick and A. N. Redlich. Towards a Theory of Early Visual Processing. *Neural Computation*, 2(3):308–320, Sept. 1990.

3. A. M. Bastos, W. M. Usrey, R. A. Adams, G. R. Mangun, P. Fries, and K. J. Friston. Canonical Microcircuits for Predictive Coding. *Neuron*, 76(4):695–711, Nov. 2012.

4. K. L. Briggman, M. Helmstaedter, and W. Denk. Wiring specificity in the direction-selectivity circuit of the retina. *Nature*, 471(7337):183–188, Mar. 2011.

5. N. Brunel. Is cortical connectivity optimized for storing information? *Nature Neuroscience*, 19(5):749–755, May 2016.

6. E. Bullmore and O. Sporns. The economy of brain network organization. *Nature Reviews Neuroscience*, 13(5):336–349, May 2012.

7. S. J. C. Caron, V. Ruta, L. F. Abbott, and R. Axel. Random convergence of olfactory inputs in the *Drosophila* mushroom body. *Nature*, 497(7447):113–117, May 2013.

8. M. Chalk, O. Marre, and G. Tkačik. Toward a unified theory of efficient, predictive, and sparse coding. *Proceedings of the National Academy of Sciences*, page 201711114, Dec. 2017.

9. J. Chapeton, T. Fares, D. LaSota, and A. Stepanyants. Efficient associative memory storage in cortical circuits of inhibitory and excitatory neurons. *Proceedings of the National Academy of Sciences*, 109(51):E3614–E3622, Dec. 2012.

10. C. Cherniak. Component placement optimization in the brain. *Journal of Neuroscience*, 14(4):2418–2427, Apr. 1994.

11. C. Cherniak, Z. Mokhtarzada, R. Rodriguez-Esteban, and K. Changizi. Global optimization of cerebral cortex layout. *Proceedings of the National Academy of Sciences*, 101(4):1081–1086, Jan. 2004.

12. R. Cohn, I. Morantte, and V. Ruta. Coordinated and Compartmentalized Neuromodulation Shapes Sensory Processing in Drosophila. *Cell*, 163(7):1742–1755, Dec. 2015.

13. H. Cuntz, F. Forstner, A. Borst, and M. Häusser. One Rule to Grow Them All: A General Theory of Neuronal Branching and Its Practical Application. *PLOS Computational Biology*, 6(8):e1000877, Aug. 2010.

14. H. Cuntz, A. Mathy, and M. Häusser. A scaling law derived from optimal dendritic wiring. *Proceedings of the National Academy of Sciences of the United States of America*, 109(27):11014–11018, July 2012.

15. S. Denève and C. K. Machens. Efficient codes and balanced networks. *Nature Neuroscience*, 19(3):375–382, Mar. 2016.

16. N. S. Desai, R. H. Cudmore, S. B. Nelson, and G. G. Turrigiano. Critical periods for experience-dependent synaptic scaling in visual cortex. *Nature Neuroscience*, 5(8):783–789, Aug. 2002.

17. R. Durbin and G. Mitchison. A dimension reduction framework for understanding cortical maps. *Nature*, 343(6259):644–647, Feb. 1990.

18. K. Eichler, F. Li, A. Litwin-Kumar, Y. Park, I. Andrade, C. M. Schneider-Mizell, T. Saumweber, A. Huser, C. Eschbach, B. Gerber, R. D. Fetter, J. W. Truman, C. E. Priebe, L. F. Abbott, A. S. Thum, M. Zlatic, and A. Cardona. The complete connectome of a learning and memory centre in an insect brain. *Nature*, 548(7666):175–182, Aug. 2017.

19. S. Gerhard, I. Andrade, R. D. Fetter, A. Cardona, and C. M. Schneider-Mizell. Conserved neural circuit structure across Drosophila larval development revealed by comparative connectomics. *eLife*, 6:e29089, Oct. 2017.

20. A. Goel, B. Jiang, L. W. Xu, L. Song, A. Kirkwood, and H.-K. Lee. Cross-modal regulation of synaptic AMPA receptors in primary sensory cortices by visual experience. *Nature Neuroscience*, 9(8):1001–1003, Aug. 2006.

21. C. P. Goold and R. A. Nicoll. Single-Cell Optogenetic Excitation Drives Homeostatic Synaptic Depression. *Neuron*, 68(3):512–528, Nov. 2010.

22. W. B. Grueber, L. Y. Jan, and Y. N. Jan. Tiling of the Drosophila epidermis by multidendritic sensory neurons. *Development (Cambridge, England)*, 129(12):2867–2878, June 2002.

23. K. N. Hartman, S. K. Pal, J. Burrone, and V. N. Murthy. Activity-dependent regulation of inhibitory synaptic transmission in hippocampal neurons. *Nature Neuroscience*, 9(5):642–649, May 2006.

24. M. Heisenberg. Mushroom body memoir: from maps to models. *Nature Reviews Neuroscience*, 4(4):266–275, Apr. 2003.

25. M. Helmstaedter, K. L. Briggman, S. C. Turaga, V. Jain, H. S. Seung, and W. Denk. Connectomic reconstruction of the inner plexiform layer in the mouse retina. *Nature*, 500(7461):168–174, Aug. 2013.

26. K. B. Hengen, M. E. Lambo, S. D. Van Hooser, D. B. Katz, and G. G. Turrigiano. Firing rate homeostasis in visual cortex of freely behaving rodents. *Neuron*, 80(2):335–342, Oct. 2013.

27. T. Hige, Y. Aso, M. Modi, G. Rubin, and G. Turner. Heterosynaptic Plasticity Underlies Aversive Olfactory Learning in Drosophila. *Neuron*, 88(5):985–998, Dec. 2015.

28. J. J. Hopfield. Neural networks and physical systems with emergent collective computational abilities. *Proceedings of the National Academy of Sciences*, 79(8):2554–2558, Apr. 1982.

29. G. S. Jefferis, E. C. Marin, R. F. Stocker, and L. Luo. Target neuron prespecification in the olfactory map of Drosophila. *Nature*, 414(6860):204–208, Nov. 2001.

30. A. Joseph and G. G. Turrigiano. All for One But Not One for All: Excitatory Synaptic Scaling and Intrinsic Excitability Are Coregulated by CaMKIV, Whereas Inhibitory Synaptic Scaling Is Under Independent Control. *The Journal of Neuroscience: The Official Journal of the Society for Neuroscience*, 37(28):6778–6785, July 2017.

31. H. Kasai, M. Matsuzaki, J. Noguchi, N. Yasumatsu, and H. Nakahara. Structure-stability-function relationships of dendritic spines. *Trends in Neurosciences*, 26(7):360–368, July 2003.

32. H. Keshishian, A. Chiba, T. N. Chang, M. S. Halfon, E. W. Harkins, J. Jarecki, L. Wang, M. Anderson, S. Cash, M. E. Halpern, and J. Johansen. Cellular mechanisms governing synaptic development in Drosophila melanogaster. *Journal of Neurobiology*, 24(6):757–787, 1993.

33. V. Kilman, M. C. W. v. Rossum, and G. G. Turrigiano. Activity Deprivation Reduces Miniature IPSC Amplitude by Decreasing the Number of Postsynaptic GABAA Receptors Clustered at Neocortical Synapses. *Journal of Neuroscience*, 22(4):1328–1337, Feb. 2002.

34. K. Krishnamurthy, A. M. Hermundstad, T. Mora, A. M. Walczak, and V. Balasubramanian. Disorder and the neural representation of complex odors: smelling in the real world. *bioRxiv*, page 160382, July 2017.

35. S. Laughlin. A simple coding procedure enhances a neuron's information capacity. *Zeitschrift Fur Naturforschung. Section C, Biosciences*, 36(9-10):910–912, Oct. 1981.

36. T. Lee, A. Lee, and L. Luo. Development of the Drosophila mushroom bodies: sequential generation of three distinct types of neurons from a neuroblast. *Development*, 126(18):4065–4076, Sept. 1999.

37. H.-H. Lin, J. S.-Y. Lai, A.-L. Chin, Y.-C. Chen, and A.-S. Chiang. A Map of Olfactory Representation in the Drosophila Mushroom Body. *Cell*, 128(6):1205–1217, Mar. 2007.

38. A. Litwin-Kumar, K. D. Harris, R. Axel, H. Sompolinsky, and L. F. Abbott. Optimal Degrees of Synaptic Connectivity. *Neuron*, 93(5):1153–1164.e7, Mar. 2017.

39. A. Maffei, S. B. Nelson, and G. G. Turrigiano. Selective reconfiguration of layer 4 visual cortical circuitry by visual deprivation. *Nature Neuroscience*, 7(12):1353–1359, Dec. 2004.

40. D. Marr. A theory of cerebellar cortex. *The Journal of Physiology*, 202(2):437–470, June 1969.

41. P. Mombaerts, F. Wang, C. Dulac, S. K. Chao, A. Nemes, M. Mendelsohn, J. Edmondson, and R. Axel. Visualizing an Olfactory Sensory Map. *Cell*, 87(4):675–686, Nov. 1996.

42. M. Murthy, I. Fiete, and G. Laurent. Testing odor response stereotypy in the Drosophila mushroom body. *Neuron*, 59(6):1009–1023, Sept. 2008.

43. S. Paradis, S. T. Sweeney, and G. W. Davis. Homeostatic control of presynaptic release is triggered by postsynaptic membrane depolarization. *Neuron*, 30(3):737–749, June 2001.

44. U. Pereira and N. Brunel. Attractor Dynamics in Networks with Learning Rules Inferred from In Vivo Data. *Neuron*, 99(1):227–238.e4, July 2018.

45. C. C. H. Petersen, R. C. Malenka, R. A. Nicoll, and J. J. Hopfield. All-or-none potentiation at CA3-CA1 synapses. *Proceedings of the National Academy of Sciences*, 95(8):4732–4737, Apr. 1998.

46. W. Rall. Branching dendritic trees and motoneuron membrane resistivity. *Experimental Neurology*, 1(5):491–527, Nov. 1959.

47. K. J. Ressler, S. L. Sullivan, and L. B. Buck. Information coding in the olfactory system: Evidence for a stereotyped and highly organized epitope map in the olfactory bulb. *Cell*, 79(7):1245–1255, Dec. 1994.

48. S. Srinivasan, R. J. Greenspan, C. F. Stevens, and D. Grover. Deep(er) Learning. *Journal of Neuroscience*, 38(34):7365–7374, Aug. 2018.

49. C. F. Stevens. What the fly's nose tells the fly's brain. *Proceedings of the National Academy of Sciences*, 112(30):9460–9465, July 2015.

50. S.-y. Takemura, Y. Aso, T. Hige, A. Wong, Z. Lu, C. S. Xu, P. K. Rivlin, H. Hess, T. Zhao, T. Parag, S. Berg, G. Huang, W. Katz, D. J. Olbris, S. Plaza, L. Umayam, R. Aniceto, L.-A. Chang, S. Lauchie, O. Ogundeyi, C. Ordish, A. Shinomiya, C. Sigmund, S. Takemura, J. Tran, G. C. Turner, G. M. Rubin, and L. K. Scheffer. A connectome of a learning and memory center in the adult Drosophila brain. *eLife*, 6:e26975, July 2017.

51. M. Tripodi, J. F. Evers, A. Mauss, M. Bate, and M. Landgraf. Structural Homeostasis: Compensatory Adjustments of Dendritic Arbor Geometry in Response to Variations of Synaptic Input. *PLOS Biology*, 6(10):e260, Oct. 2008.

52. G. Turrigiano. Homeostatic Synaptic Plasticity: Local and Global Mechanisms for Stabilizing Neuronal Function. *Cold Spring Harbor Perspectives in Biology*, 4(1):a005736, Jan. 2012.

53. G. G. Turrigiano, K. R. Leslie, N. S. Desai, L. C. Rutherford, and S. B. Nelson. Activity-dependent scaling of quantal amplitude in neocortical neurons. *Nature*, 361:892–896, Feb. 1998.

54. C. Vale and D. H. Sanes. The effect of bilateral deafness on excitatory and inhibitory synaptic strength in the inferior colliculus. *European Journal of Neuroscience*, 16(12):2394–2404, Dec. 2002.

55. C. van Vreeswijk and H. Sompolinsky. Chaos in neuronal networks with balanced excitatory and inhibitory activity. *Science (New York, N.Y.)*, 274(5293):1724–1726, Dec. 1996.

56. D. I. Vaney, B. Sivyer, and W. R. Taylor. Direction selectivity in the retina: symmetry and asymmetry in structure and function. *Nature Reviews Neuroscience*, 13(3):194–208, Mar. 2012.

57. R. Vassar, S. K. Chao, R. Sitcheran, J. M. Nun˜ez, L. B. Vosshall, and R. Axel. Topographic organization of sensory projections to the olfactory bulb. *Cell*, 79(6):981–991, Dec. 1994.

58. L. B. Vosshall, A. M. Wong, and R. Axel. An Olfactory Sensory Map in the Fly Brain. *Cell*, 102(2):147–159, July 2000.

59. F. Wang, A. Nemes, M. Mendelsohn, and R. Axel. Odorant Receptors Govern the Formation of a Precise Topographic Map. *Cell*, 93(1):47–60, Apr. 1998.

60. M. Weigand, F. Sartori, and H. Cuntz. Universal transition from unstructured to structured neural maps. *Proceedings of the National Academy of Sciences*, 114(20):E4057–E4064, May 2017.

Supplementary Figures

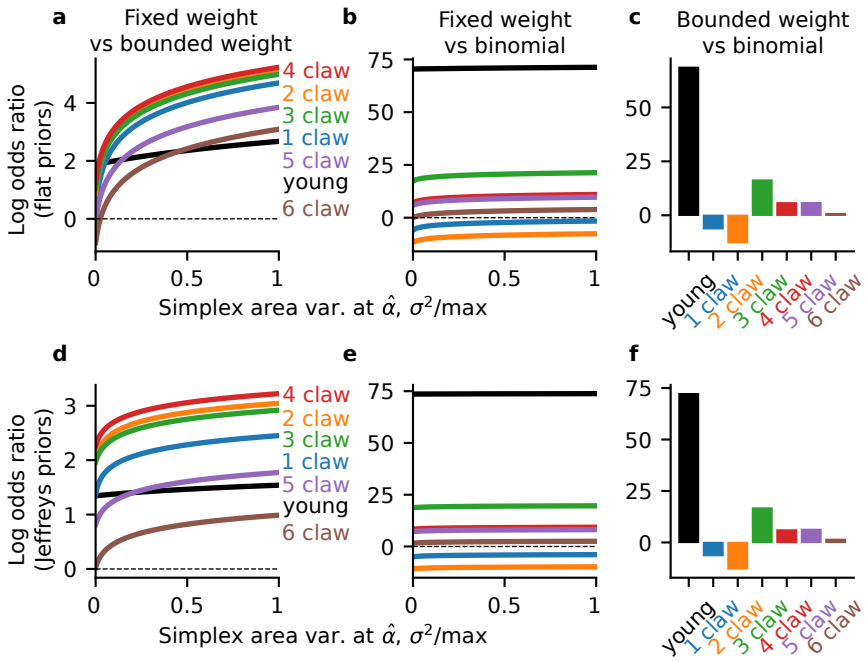

Fig 8. Log odds ratios for larval Kenyon cell input degrees. (**a**) Log posterior odds ratio for the simplex area distribution vs the simplex volume distribution, under a flat prior for the parameter α. All posterior odds are computed by the Laplace approximation—a gaussian approximation for the likelihood in α. The Laplace approximation yields point estimates of the posterior odds for the simplex volume and zero-truncated binomial models (Methods: 6.9, 6.11). For the simplex area model, this yields lower and upper bounds for the posterior odds (Methods: 6.6). Those bounds are parameterized by the variance of that gaussian, σ_α^2. For each cell type, we varied σ_α^2 between its lower and upper bounds and computed the posterior odds at each σ_α^2. Since those bounds differ between cell types, we normalized them to compare the odds ratios. (**b**) Same as a), for the simplex area vs the zero-truncated binomial model. (**c**) Posterior odds ratio for the simplex volume vs the zero-truncated binomial model. (**d-f**) Same as (a-c), but with the Poisson Jeffreys prior for α, $p(\alpha) \propto 1/\sqrt{\sigma}$.

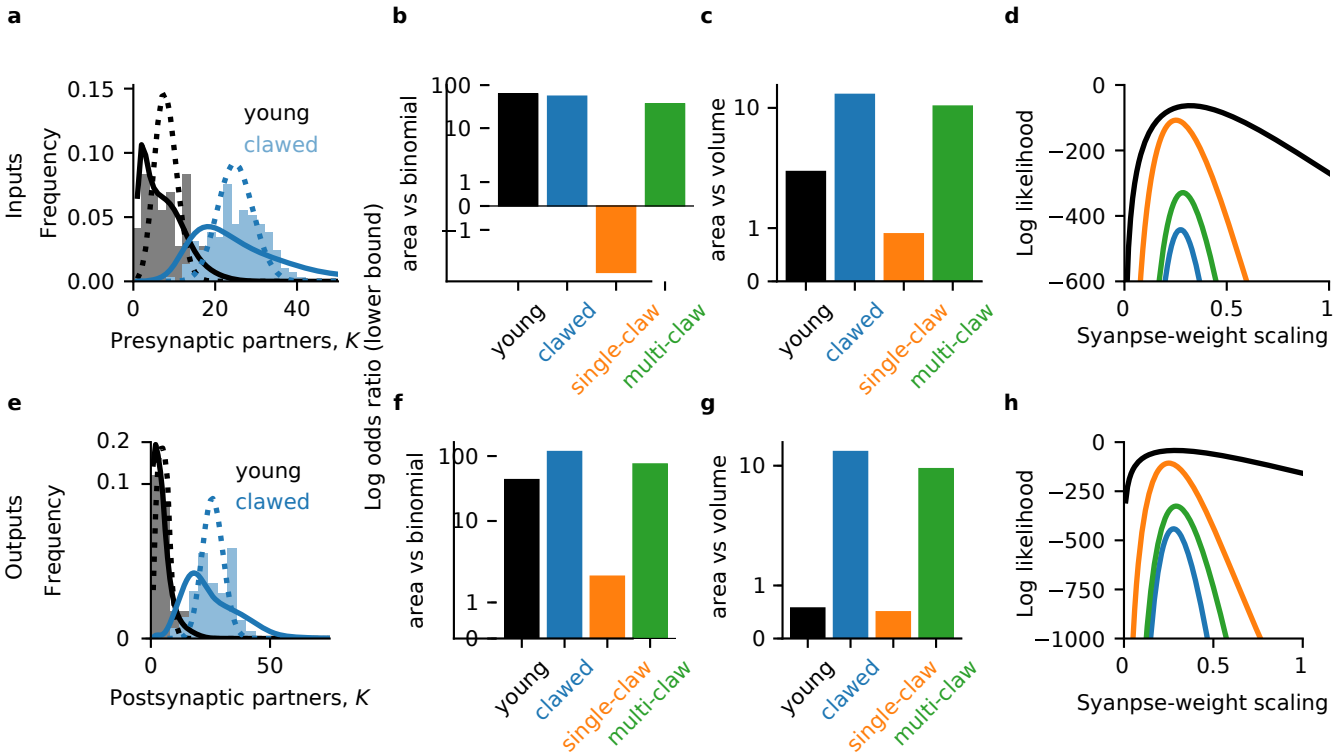

Fig 9. Larval Kenyon cell axo-axonal connectivity. (**a**) Input degree distributions for larval KCs. (**b**) Log odds ratio for the fixed net weight model vs the binomial wiring model. (**c**) Log odds ratio for the fixed net weight model vs bounded net weight model. (**d**) Likelihood as a function of the synapse-weight scaling parameter α. **e-h**) Same as (**a-d**) for KC axo-axonal outputs.

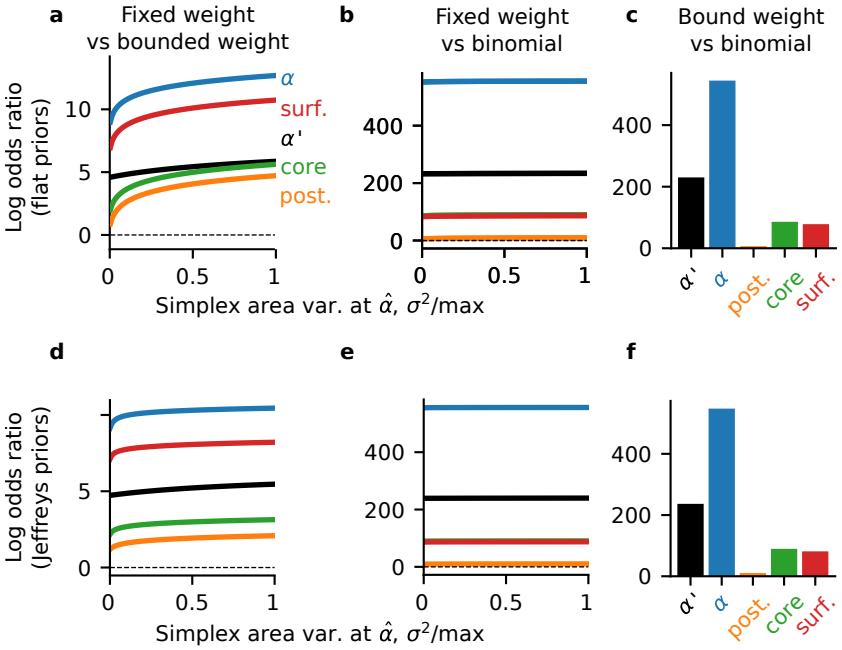

Fig 10. Log odds ratios for adult Kenyon cell input degrees. Same as Supp. Fig. 8, but for adult Kenyon cells.

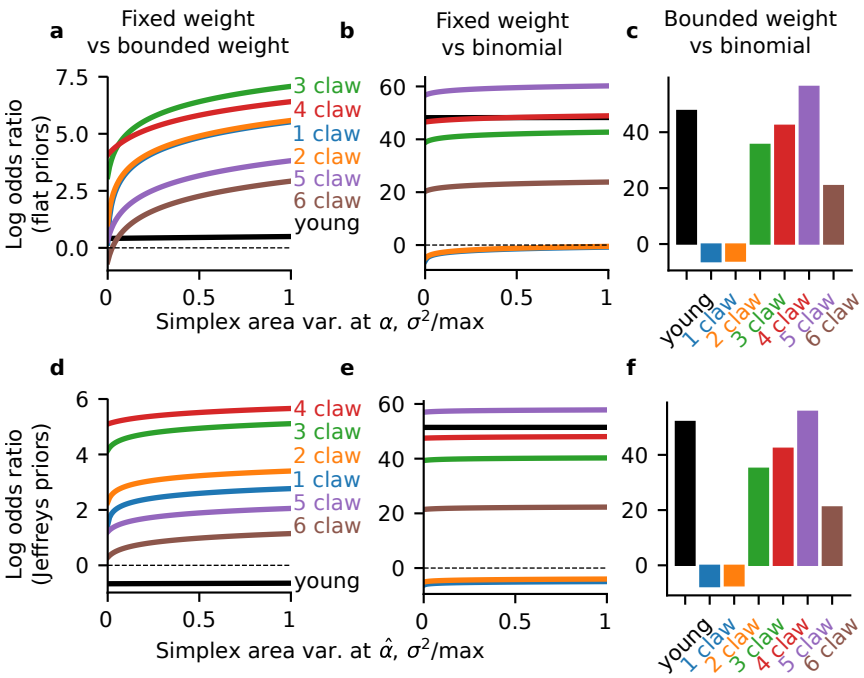

Fig 11. Log odds ratios for larval Kenyon cell output degrees. Same as Supp. Fig. 8, but for larval Kenyon cell outputs.

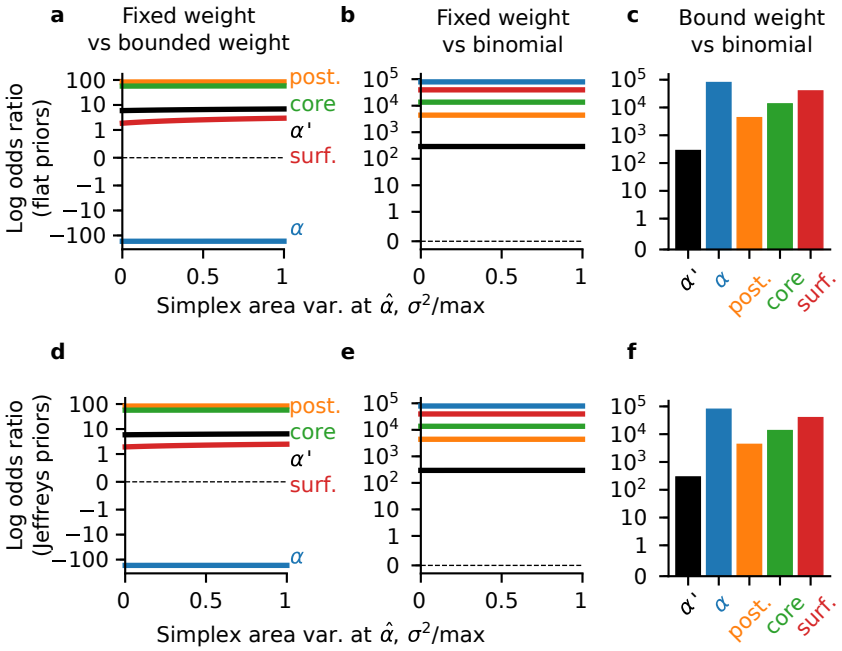

Fig 12. Log odds ratios for adult Kenyon cell output degrees. Same as Supp. Fig. 8, but for adult Kenyon cell outputs.

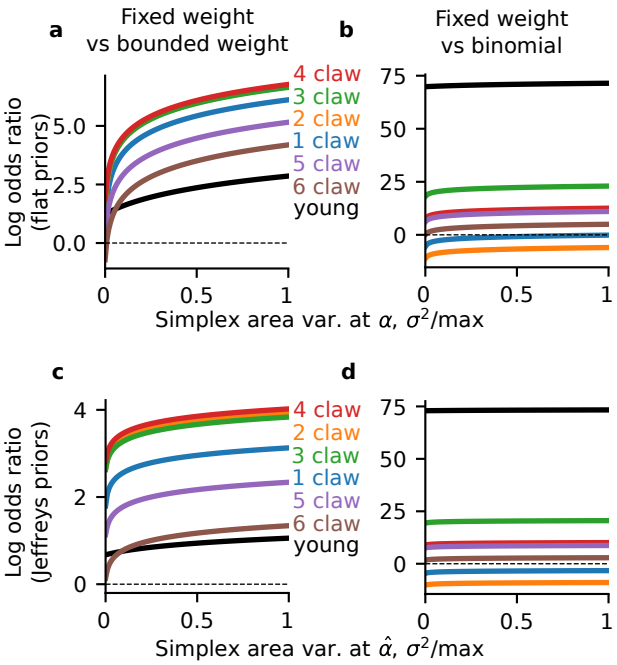

Fig 13. Log odds ratios for larva Kenyon cell input degrees with 1-norm surface area model. Same as Supp. Fig. 8, but for the 1-norm simplex surface area model (Methods: 6.4).

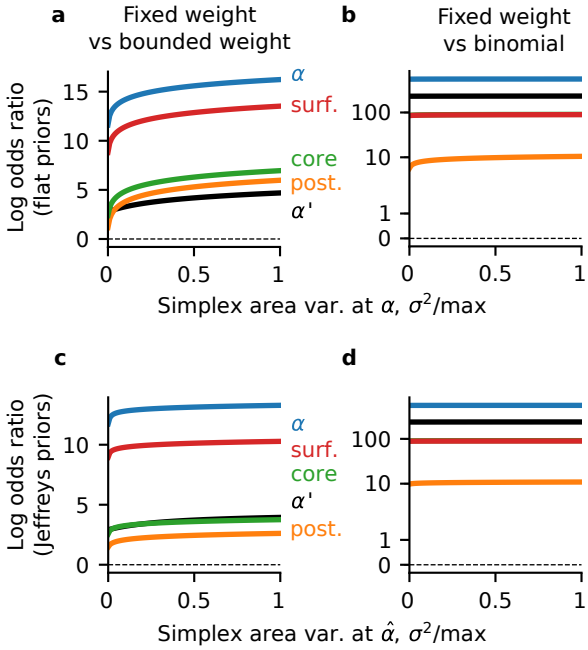

Fig 14. Log odds ratios for adult Kenyon cell input degrees with 1-norm surface area model. Same as Supp. Fig. 10, but for the 1-norm simplex surface area model (Methods: 6.4).

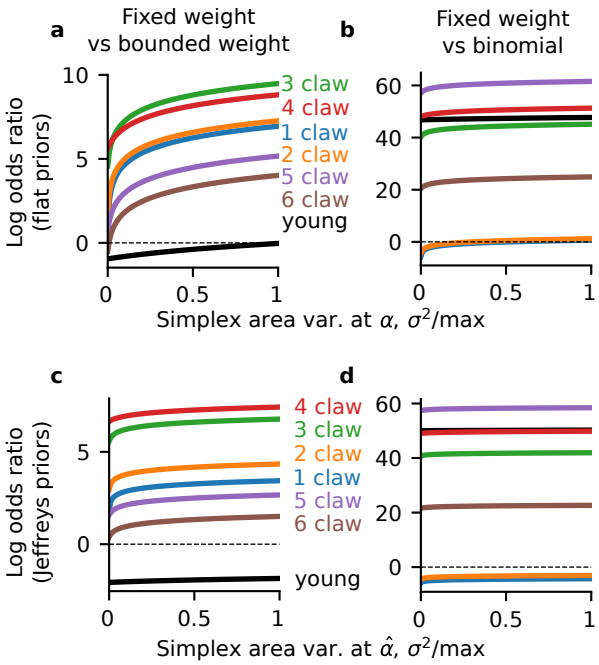

Fig 15. Log odds ratios for larva Kenyon cell output degrees with 1-norm surface area model. Same as Supp. Fig. 11, but for the 1-norm simplex surface area model (Methods: 6.4).

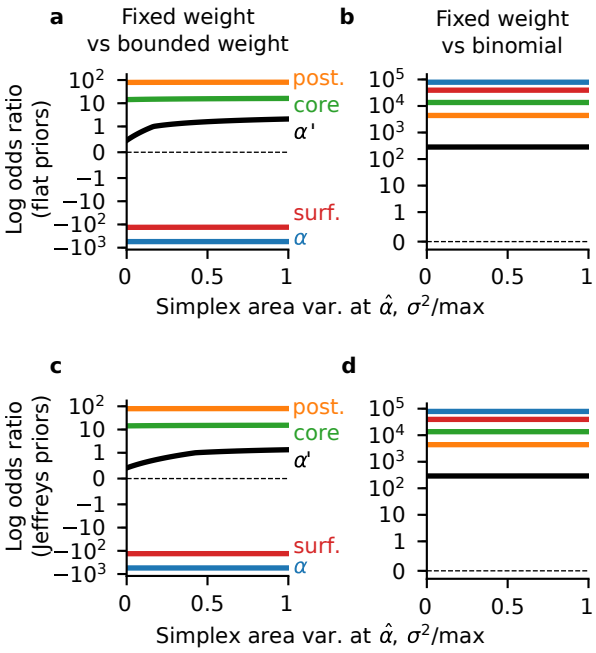

Fig 16. Log odds ratios for adult Kenyon cell output degrees with 1-norm surface area model. Same as Supp. Fig. 12, but for the 1-norm simplex surface area model (Methods: 6.4).